JOURNAL OF GEOPHYSICAL RESEARCH, VOL. 105, NO. E5, PAGES 12,035–12,052, MAY 25, 2000

Localization of bedding plane slip and backthrust faults above blind thrust faults: Keys to wrinkle ridge structure

Richard A. Schultz
Geomechanics–Rock Fracture Group, Department of Geological Sciences, Mackay School of Mines, University of Nevada, Reno

Abstract. A mechanically based model for wrinkle ridge development is developed that combines wrinkle ridge morphologies, regional topographic offsets suggestive of subsurface thrust faults, and folding of near-surface layers. This model provides explicit relationships between observed morphologic elements characteristic of wrinkle ridges and plausible mechanisms in the subsurface, a key component that is absent in previous qualitative fault-based scenarios for these structures. As developed in this paper, wrinkle ridges are the surface expression of anticlines that grow above a blind thrust fault as a result of both flexural slip folding of near-surface strata and the nucleation and growth of echelon arrays of backthrust faults. Calculations of displacements (both horizontal shortening and vertical uplift) and Coulomb stress change related to slip along blind thrust faults in the model demonstrate physically important spatial inhomogeneities in these quantities, with revealing and useful implications. (1) The ratio of shortening due to folding at the surface to the shortening due to faulting at depth is characteristically small for coupled wrinkle ridge-blind thrust fault systems and decreases with increasing fault depth; the depth of the blind thrust fault's upper tip thus profoundly influences the surface strains. (2) Folding and uplifted topography, forming the topographic ridge, are produced above the area of the slipping blind thrust fault plane. Horizontal and vertical deformation at the surface extend over several ridge widths, or a total of at least 50 km for a 10-km–wide ridge, implying that topographic profiles and geologic studies must extend sufficiently far from the wrinkle ridge to fully characterize the surface deformation. (3) Calculations of Coulomb stress changes suggest that fault slip can localize both bedding plane slip in overlying strata and new backthrust faults that propagate upward to become wrinkles on the trailing side of the ridge. Initiation of bedding plane slip in association with slip along the blind thrust fault likely determines whether the resulting surface structure becomes a wrinkle ridge or a lobate scarp. Wrinkle ridge spacing may also be related to stress changes associated with slip along the underlying blind thrust fault.

1. Introduction

Wrinkle ridges are probably one of the most commonly observed, yet least understood, classes of planetary structures. Numerous previous studies have documented their appearance [e.g., *Strom*, 1972; *Lucchitta*, 1976], dimensions [e.g., *Watters*, 1988], contractional strain significance [e.g., *Howard and Muehlberger*, 1973; *Lucchitta*, 1977; *Plescia and Golombek*, 1986; *Sharpton and Head*, 1988; *Golombek et al.*, 1991; *Banerdt et al.*, 1992; *Mangold et al.*, 1998], and occurrences on terrestrial planets including Mercury [e.g., *Strom et al.*, 1975], Venus [e.g., *Kreslavsky and Basilevsky*, 1998; *Bilotti and Suppe*, 1999], Earth [*Plescia and Golombek*, 1986; *Watters*, 1988], Moon [e.g., *Lucchitta*, 1976, 1977; *Sharpton and Head*, 1988], and Mars [e.g., *Plescia*, 1991, 1993; *Watters and Robinson*, 1997]. Many conceptual, kinematic, and mechanical models have been created and applied to better interpret the morphologies and geodynamic significance of wrinkle ridges. However, several critical aspects of wrinkle ridge morphology and development remain unresolved, leading to substantial disagreement over fundamental issues, such as the relative roles of folding and faulting in wrinkle ridge growth, depth extent, and quantitative implications for regional deformation and strain magnitude [e.g., *Tanaka et al.*, 1991; *Zuber*, 1995].

The problem of wrinkle ridge development can now be tackled from a fresh perspective in light of new and intriguing results for terrestrial blind thrust faults (that interact with but do not break the surface). That work [e.g., *Cooke and Pollard*, 1997; *Roering et al.*, 1997; *Niño et al.*, 1998] has demonstrated the importance of localization processes on fault-related deformation that have not been considered or emphasized previously in the context of planetary anticline or wrinkle ridge growth. As discussed and demonstrated below, both localization of bedding plane slip above the blind fault tip, and creation of new antithetic backthrust faults, by slip along the subjacent blind thrust fault hold considerable promise as mechanisms for relating surface morphology to subsurface processes, and thereby to larger-scale geodynamics.

In this paper I develop a mechanical model for the inception of wrinkle ridges that is based on the surface deformation predicted to occur in response to a blind thrust fault located at some depth beneath the planetary surface. The mechanical model has the potential to explicitly and systematically relate surface morphology to the geometry and characteristics of subsurface faulting, something previous conceptual hypotheses that invoked thrust faulting were unable to accomplish, given their purely qualitative natures.

Despite a rather extensive literature on both wrinkle ridge phenomena and the mechanics of faulting, few studies have attempted

Paper number 1999JE001212.
0148–0227/00/1999JE001212$9.00

to explicitly relate the two. Given the depth of knowledge in both separate fields, along with recent rapid developments in both, this paper is necessarily rather lengthy. The paper is structured as follows:

1. First, I briefly summarize the morphology of wrinkle ridges, highlighting both what is known and what is still ambiguous despite several decades of study.

2. Next, the central role of stratigraphy in promoting wrinkle ridge morphologies is outlined, revealing that flexural slip folding of layered sequences appears to be required for wrinkle ridges to grow.

3. Previous structural models for wrinkle ridges are reviewed next and critically evaluated, followed by a new quantitative test of wrinkle ridge morphometry, using balanced kinematic constructions, that demonstrates that these structures are consistent with the surface expression of folds. At this point in the paper, we can demonstrate that wrinkle ridges mostly likely formed as flexural slip folds above thrust faults that do not sole into a basal décollement, which itself represents a substantial advance over preceding studies.

4. In section 6, new results from intensive independent study of terrestrial blind thrust faults are presented as they pertain to planetary wrinkle ridges. In particular, the coupled interaction between faulting and folding (of the strata overlying the fault) demonstrates the intractability of separately assessing these two related processes, as has been debated and attempted in the past.

5. The preceding body of work, presented in necessary detail in the previous sections, motivates and defines a new synoptic structural model for wrinkle ridges that is presented next. This mechanically based model contrasts with previous qualitative fault-based scenarios contained in the literature that lack a firm physical basis or predictive capability for wrinkle ridge morphology.

6. A suite of calculations is presented in section 7 that exploits the initial conditions of wrinkle ridge development (i.e., displacement along a blind thrust fault beneath the surface) to illustrate key principles that are important in interpreting wrinkle ridges for the subsurface structure. These representative calculations lay the groundwork for physically interpreting long-held observations such as the ratio of folding to faulting strains, surface displacements, and the morphologic transition between wrinkle ridges and their structural cousins, lobate scarps.

2. Wrinkle Ridge Morphology

Wrinkle ridges can be described by two principal elements (Figure 1a): a broad ridge (called the "mare ridge" for lunar examples) up to tens of kilometers wide and meters to kilometers high; and sinuous, discontinuous, or echelon crenulations ("wrinkles") located on or near the ridge [e.g., *Maxwell et al.*, 1975; *Schultz*, 1976, pp. 308–337; *Lucchitta*, 1977; *Lucchitta and Klockenbrink*, 1981; *Sharpton and Head*, 1988; *Watters*, 1988]. Ridges can vary from gentle, nearly undetectable swells to prominent, asymmetric rises bounded on one or both sides by scarps. Wrinkles are typically found near a ridge's margin (Figures 1a, 1b, and 1c), although they also can occur at its top (Figure 1d) or in the surrounding plains. In many cases the wrinkle is found where the asymmetric ridge is highest [*Lucchitta*, 1977; *Watters*, 1988; *Golombek et al.*, 1991; *Watters and Robinson*, 1997] (Figure 1b). Observations of the margins of both wrinkles and ridges are consistent with thrust faulting, with wrinkles defining fault surfaces antithetic to the main fault beneath the ridge [e.g., *Howard and Muehlberger*, 1973; *Sharpton and Head*, 1988; *Mangold et al.*, 1998].

The terminology associated with wrinkle ridges, such as that used above, is not universally agreed upon. Many authors include a third topographic element, a broad, low-relief arch, on which the wrinkle ridge is sometimes, but not always, developed or even associated [e.g., *Strom*, 1972; *Sharpton and Head*, 1988; *Golombek et al.*, 1991]. For example, *Colton et al.* [1972] broke from previous interpretations [e.g., *Strom*, 1972] by inferring that the lunar wrinkle ridges in southern Oceanus Procellarum that they studied were not related to the morphologically distinct arches, suggesting different origins for those wrinkle ridges and arches (see their Figure 29-125). Indeed, many arches that are associated only spatially (by simple proximity, and regardless of trend) with wrinkle ridges may not even be genetically related to them. *Strom* [1972] and others have interpreted some lunar arches as laccoliths (see review by *Sharpton and Head* [1988] for other volcanic hypotheses for arch formation), a mechanism that was supported by *Colton et al.*'s [1972] observations of crestal fractures on the arches (but not on the separate wrinkle ridges).

In another approach, *Watters* [1988] used the arch-and-ridge terminology to describe different scales of wrinkle ridge morphology using his preferred model of first-, second-, and third- order folds (e.g., the lobate edge labeled "R" in Figure 1a was considered the arch by *Watters* [1988]). *Golombek et al.* [1991] retained the arch concept (called the "broad rise" by them) yet combined it with the ridge (their "superimposed hill") in their fault-based concept of wrinkle-ridge topography. As a result, substantial ambiguity exists both in interpreting the origin of arches, ridges, and wrinkles, and in relating them mechanically to wrinkle ridges in a self-consistent and informative manner. This paper focuses on formation of the ridge and wrinkles (as defined here and following *Colton et al.* [1972]), given that definitive and systematic relationships between wrinkle ridges and arches (as used in the literature) are not yet available.

3. Interactions With Stratigraphy

Previous studies have concluded that strength contrasts between shallow stratigraphic layers are important in the formation or morphology of wrinkle ridges [e.g., *Muehlberger*, 1974; *Plescia and Golombek*, 1986; *Sharpton and Head*, 1988; *Watters*, 1988, 1991, 1993; *Golombek et al.*, 1991; *Mangold*, 1997; *Mangold et al.*, 1998]. For example, most of the classic cases of potential terrestrial analogs reported by *Plescia and Golombek* [1986] (e.g., El Asnam [*King and Yielding*, 1984], Columbia Plateau basalts [*Reidel et al.*, 1989; *Watters*, 1989; *West et al.*, 1996], Buena Vista Hills, Alae basalt-filled crater, Palos Verdes Hills) are formed in layered sequences. Impact craters or multiring basins that are buried by various stratigraphic units contribute to the morphology and patterns of wrinkle ridges [e.g., *Lucchitta*, 1977; *Schultz et al.*, 1982; *Chicarro et al.*, 1985; *Schultz and Frey*, 1990; *Watters*, 1993; *Kreslavsky and Basilevsky*, 1998; *Mangold et al.*, 1998], supporting inferences that near-surface layers, mechanical discontinuities, or slipping décollements (as opposed to deeper structures) can locally control wrinkle ridge growth (see also *Sharpton and Head* [1988] for comparable conclusions and supporting documentation).

Morphologic investigations of wrinkle ridges demonstrate that they are the surface expression of folds [*Howard and Muehlberger*, 1973; *Plescia and Golombek*, 1986; *Watters*, 1988]. Folding of a sequence of rocks is favored over throughgoing faulting, for example, either when large strength contrasts between layers exist or by the presence of numerous potential slip surfaces, such as bedding planes, within the sequence [*Johnson*, 1980; *Erickson*, 1996].

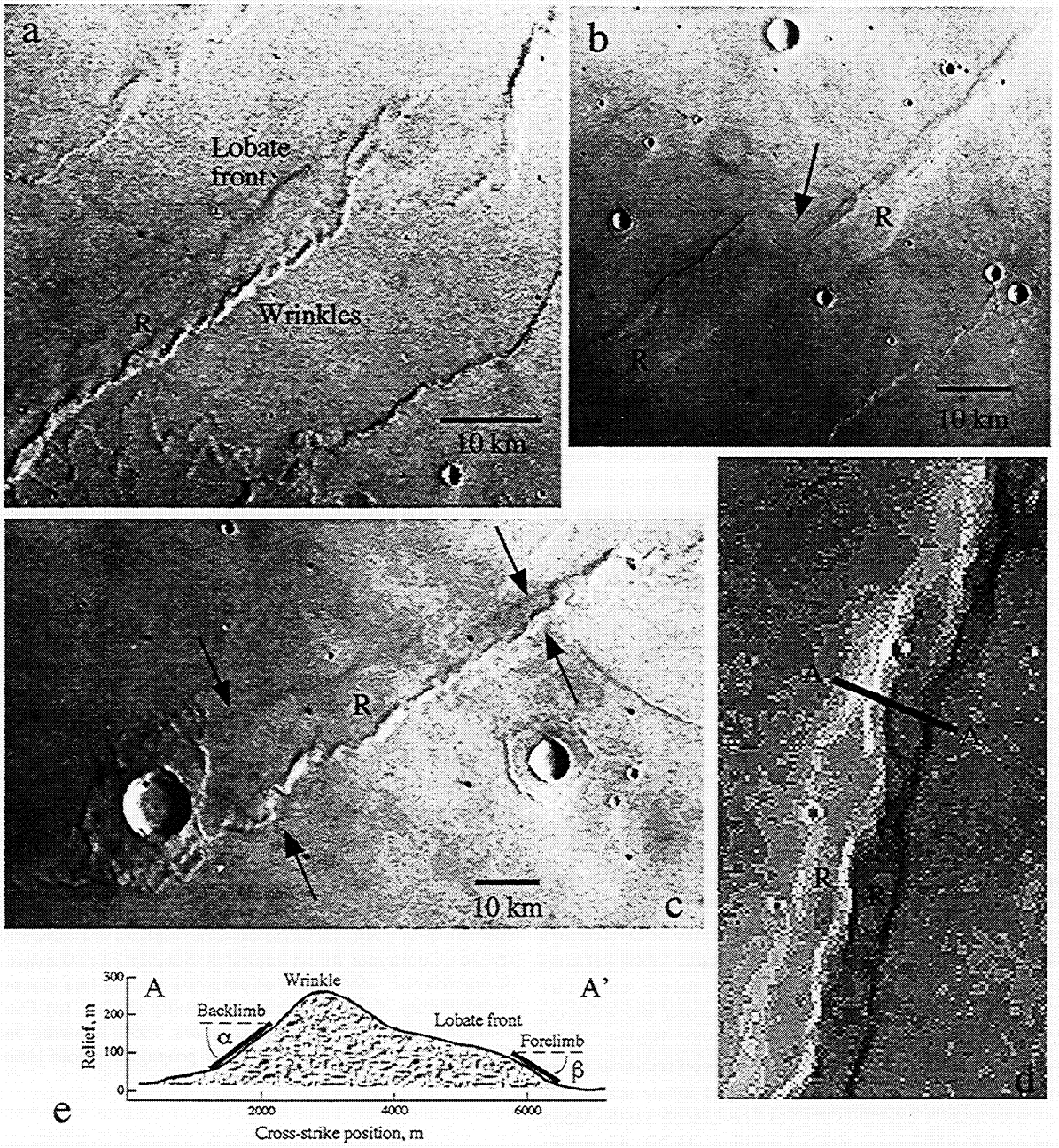

Figure 1. Examples of wrinkle ridge structures from Sinai Planum region (Figures 1a–1c) of Mars. The main ridge antiform is indicated by "R." (a) Wrinkle ridge (Viking orbiter image 608A45) located near 23°S, 79° showing lobate ridge front and wrinkles (echelon backthrust faults). North is toward upper right; vergence is east to west. (b) Echelon ridge showing lateral ramp (arrow) developed between wrinkles and ridges [after *Mangold et al.*, 1998] (Viking image 608A44) near 21°S, 83°. North is toward upper right; vergence is west to east. (c) Wrinkle ridge showing decrease in ridge width along strike (arrows) toward termination (upper right part of frame, Viking image 608A65, near 19°S, 84°). North is toward upper right; vergence is east to west. (d) Wrinkle ridge in Lunae Planum near 22°N, 62° with echelon wrinkles located along center of ridge (Viking image 520A25) showing location of topographic profile A–A' [*Watters and Robinson*, 1997] given in Figure 1e. (e) Measured topography of wrinkle ridge (Figure 1d), after *Watters and Robinson* [1997]. Profile length is ~5 km, showing backlimb and forelimb angles.

In general, sedimentary or volcanic layering (e.g., interbedded basalt flows) is one type of mechanical stratification; other mechanisms that can create mechanical anisotropy include fracturing, planar segregation of igneous or metamorphic minerals, temperature contrasts (e.g., volcanic cooling units), permafrost and ground ice development, and chemical precipitation. To the extent that these other forms of stratification promote the development of flexural slip folds, they may be possible contributors to wrinkle ridge structure. In this paper, "layering" refers to any type of stratification that is associated with mechanically significant contrasts in material properties or strengths between layers. Although folding can occur in massive units (e.g., soils) by continuum flow mechanisms

(e.g., block rotations, pressure solution, cataclasis), slip along interfaces within a layered sequence, such as bedding planes, reduces the unit's resistance to buckling or flexural deformation [e.g., *Currie et al.*, 1962; *Watters*, 1991]. Many folds exhibit a combination of mechanisms depending on the source of stress and the amplitude of folding.

Ongoing analyses of high-resolution Mars Orbiter Camera (MOC) images, acquired from the orbiting Mars Global Surveyor spacecraft, demonstrate the presence and regional extent of fine-scale layering on Mars, analogous in areas to terrestrial flood basalt sequences with sedimentary interbeds. Sequences of individual layers ~5–10 m thick can attain aggregate thicknesses exceeding 5 km in the Valles Marineris region [*Malin et al.*, 1998; *McEwen et al.*, 1999]. These new observations of widespread, fine-scale layering in the Martian crust [*Malin and Edgett*, 1999] provide a firm basis for interpreting Martian wrinkle ridges as anticlinal folds by demonstrating that stratification consistent with folding exists in many areas. Flatirons and other landforms consistent with distinct layers that were eroded and tilted were noted by *Schultz and Tanaka* [1994] above the Martian Coprates rise, interpreted by them and others as a large anticline.

4. Previous Hypotheses for Origin

Although early workers advocated a wide variety of mechanisms for wrinkle ridge formation [e.g., *Colton et al.*, 1972], an origin by localized deformation (folding and/or faulting) is most consistent with the observations [*Howard and Muehlberger*, 1973; *Lucchitta*, 1976, 1977; *Plescia and Golombek*, 1986; *Sharpton and Head*, 1988; *McGill*, 1993] (see Table 1). Intersections of ridges with impact craters [*Lucchitta*, 1976; *Sharpton and Head*, 1988; *Mangold et al.*, 1998] demonstrate that wrinkle ridges accommodate contractional strain with little or no strike-slip component. *Howard and Muehlberger* [1973] inferred that the lunar wrinkle ridges they studied grew as anticlines above subjacent thrust faults.

Many wrinkle ridges deform units interpreted to be layered lava flows [*Mouginis-Mark et al.*, 1992; *Malin et al.*, 1998] yet continue along-strike into more massive units as lobate scarps that exhibit a different surface morphology [*Howard and Muehlberger*, 1973; *Lucchitta*, 1976; *Sharpton and Head*, 1988; *Watters*, 1993; *Mangold et al.*, 1998]. The morphology and contractional strain signatures of well-studied and clearly imaged lobate scarps, including representative examples such as Lee-Lincoln on the Moon [*Howard and Muehlberger*, 1973; *Lucchitta*, 1976], Amenthes Rupes on Mars [*Watters*, 1993; *Watters and Robinson*, 1997], and Discovery Rupes on Mercury [*Watters et al.*, 1998], demonstrate that lobate scarps are surface-breaking thrust faults formed in nonlayered or nonslipping rock masses. Many wrinkle ridges on the Moon and Mars, for example, change along-strike into lobate scarps, with the change in morphologic expression related to changes in the layering properties of the underlying geologic units as noted above. This well-known morphologic change (see references above) implies that wrinkle ridges form most efficiently above thrust faults in layered (not massive) materials.

Table 1. Tectonic Hypotheses for Wrinkle Ridge Formation

Hypothesis	Primary Arguments
Buckling	periodic ridge spacing, antiformal shape
Thrust faulting	offset topography, contractional strains
Splay faults	antithetic ridge morphology
Décollements	ridge-crater intersections

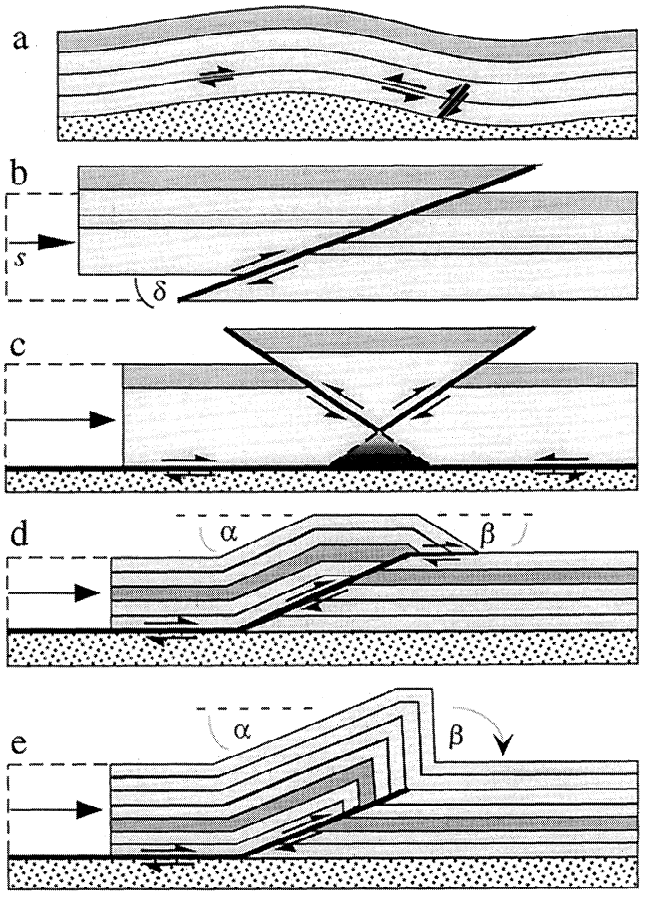

Figure 2. Structural models proposed for planetary wrinkle ridges. (a) Buckle fold showing nucleation of thrust faults within oversteepened concentric folds [*Watters*, 1988]. (b) Simple thrust fault with horizontal and vertical components of rigid body displacement related only to shortening s and fault dip angle δ; hypothetical splay faults included by some authors not shown for clarity. (c) Conjugate thrust faults [*Allemand and Thomas*, 1992; *Mangold et al.*, 1998]; area of potential overlap (the kinematic incompatibility of the geometry) is heavily shaded. (d) Fault-bend fold [*Suppe*, 1983; *Suppe and Connors*, 1992] showing backlimb dip α and forelimb dip β. (e) Fault-propagation fold [*Mercier et al.*, 1997]; α and β as in Figure 2d.

4.1. Folding-Based Models

Wrinkle ridges on Mars and other planetary bodies are commonly developed with a quasi-regular or periodic spacing [e.g., *Schultz*, 1976, pp. 334–335; *Watters*, 1989, 1991]. Combined with their anticlinal morphologies, the regular spacing has suggested that layer-parallel compression and buckling instability may have contributed to wrinkle ridge formation, spacing, and growth [*Saunders and Gregory*, 1980; *Watters*, 1991] (Table 1). In this scenario, wrinkle ridges can be interpreted as low-amplitude buckle folds [e.g., *Currie et al.*, 1962; *Muehlberger*, 1974] (Figure 2a) with a spacing inherited from the dominant wavelength of folding for the layered sequence. *Watters* [1991] found that rather large contrasts in elastic (or viscous) material properties between a capping sequence of interbedded basaltic (or similar) layers and weaker megaregolith below were required, at the time of buckling, for fold-

ing to occur instead of thrust faulting. Using the properties of jointed basaltic rock masses, *Schultz and Watters* [1995] found that buckling could occur under much smaller horizontal stresses and for much smaller values of modulus ratio. Although the dominant wavelength of folding can be related to the thickness of the surficial strong layers [*Watters*, 1991], *Zuber and Aist* [1990] demonstrated that a range of stratigraphies (i.e., with or without a megaregolith or basaltic caprock sequence) and a range of rheologies (elastic, viscous, plastic) could satisfy the observations of wrinkle ridge spacing, effectively relaxing the implied association between spacing and stratigraphy.

The buckling models suggest that the horizontal shortening strains accommodated by the buckle folds may exceed those accommodated by secondary faulting along tightened and rotated fold limbs and within the cores of the wrinkle ridge anticlines [e.g., *Watters*, 1988, 1991]. They also imply that wrinkle ridges are predominantly shallow structures, confined to the near-surface stratigraphy (upper few kilometers or less). *Watters* [1988] noted, however, that a buckling model was not intended to apply to wrinkle ridges that continue along-strike as lobate scarps, and that thrust faulting may be necessary to fully account for contractional strains measured across wrinkle ridges. A décollement surface, or layer of intervening material such as megaregolith, is implied for certain Martian stratigraphies (see *MacKinnon and Tanaka* [1989], *Zuber and Aist* [1990], and *Mangold et al.* [1998] for discussion) that could decouple the buckled upper section from deeper crust and lithosphere below. Such a decoupling would diminish the utility of observations and measurements of wrinkle ridges in providing clues to details of stress state and deformation regime at depth, which are required for geodynamic models, for example, of Tharsis development [*Tanaka et al.*, 1991; *Zuber*, 1995; *Smith et al.*, 1999].

4.2. Faulting-Based Models

Observations of wrinkle ridges that clearly deform craters along discrete curviplanar surfaces [e.g., *Sharpton and Head*, 1988; *Mangold et al.*, 1998] and that continue along-strike into massive geologic units, such as bedrock massifs, as lobate thrust fault scarps [*Howard and Muehlberger*, 1973; *Lucchitta*, 1976; *Watters*, 1993] have suggested that wrinkle ridges primarily reflect the surface expression of faults (Table 1). As used in this paper, "thrust fault" is inclusive of reverse faults by referring to the sense of displacement without specifying specific values of fault dip angle.

The simplest and most widespread faulting-based hypothesis [e.g., *Plescia and Golombek*, 1986; *Golombek et al.*, 1989, 1991; *Plescia*, 1991] involves translation of rigid crustal blocks along a shallowly dipping thrust fault having indefinite depth extent (Figure 2b). Although secondary structures are sometimes drawn artistically in the near-surface (minor folding, splays of various orientations, slip magnitudes, and slip senses [*Howard and Muehlberger*, 1973; *Golombek et al.*, 1991]; not shown in Figure 2b), no physically based mechanism is proposed in the literature that would systematically predict the characteristic wrinkle ridge morphologies. As a result, the simple faulting-based models (e.g., Figure 2b; see also *Plescia and Golombek* [1986] and *Golombek et al.* [1991]) may provide some insight into causes for suspected topographic offsets across wrinkle ridges (see below), and for qualitatively associating some obvious surface features with surface-breaking thrusts, but they are uninformative by construction for systematically interpreting how wrinkle ridges grow and what factors control their classic morphologies. *Zuber* [1995] has additionally used mechanical models to demonstrate the importance of stratigraphic variations in transmitting stresses due to thrust fault slip at depth to the surface.

A geometrically based "pop-up" model that represents a wrinkle ridge as a wedge bounded by two conjugate thrust faults nucleating simultaneously along a regional décollement has been suggested by *Allemand and Thomas* [1992] and *Mangold et al.* [1998] (Figure 2c; but note kinematic incompatibility of interpenetrating rocks implied beneath the wedge, heavily shaded). The opposing fault planes required by this model are consistent with observations of paired scarps [e.g., *Howard and Muehlberger*, 1973] that bound wrinkle ridges in deformed craters on the Moon [*Sharpton and Head*, 1988] and Mars [*Mangold et al.*, 1998]. *Mangold et al.* [1998] also argued that subcircular wrinkle ridges, which mimic the planforms of buried impact craters, are better explained by shallowly rooted faults than by deep-seated ones (see also *Sharpton and Head* [1988] and *Watters* [1993] for comparable conclusions). *Mangold et al.* [1998] suggested that shallow décollements provide a mechanism to maintain a consistent thickness of the deforming sequence in near-surface strata.

As a test of the simplest folding- and faulting-based models, *Golombek et al.* [1991] measured topographic profiles across several lunar wrinkle ridges by using available topographic contour maps produced from Lunar Orbiter data. They inferred subtle changes in topography across wrinkle ridges that were interpreted as vertical regional elevation offsets due to slip along (single) thrust faults beneath the ridges (see also *Sharpton and Head* [1988] and *Golombek et al.* [1989]). More recently, *Golombek and Banerdt* [1999] and *Golombek et al.* [1999, 2000] report preliminary topographic profiles across Martian wrinkle ridges by Mars Orbiter Laser Altimeter (MOLA) data that may be analogous in interpretation to the lunar profiles. The suggested elevation offsets were used to calculate the amount of horizontal shortening s (and inhomogeneous fault strain [*Jamison*, 1989; *Wojtal*, 1989; *Schultz*, 2000], assuming particular values for traverse line lengths) accommodated by the subjacent fault using their rigid block model (Figure 2b; the "shortening due to faulting", S_{fault}). Profiles constructed along the lunar mare surface across the wrinkle ridge were "unrolled" to also estimate the degree of shortening due to folding alone (at the lunar surface, S_{fold}; see also *Watters* [1988] and *Watters and Robinson* [1997] for similar techniques applied to folding at Martian wrinkle ridges). *Golombek et al.* [1991] found that the "shortening due to faulting" typically exceeded that "due to folding" by about an order of magnitude. Total shortening across the wrinkle ridge was determined by adding the faulting and folding components together (implicitly assuming that the two values are independent quantities). Analogous results were reported for several Martian wrinkle ridges by *Plescia* [1991, 1993].

The *Golombek et al.* [1991] model is summarized by them as follows (see also *Plescia and Golombek* [1986]):

1. If S_{fault} (at depth) $\approx S_{fold}$ (at the surface), the wrinkle ridge is a fold over a blind thrust fault. Fault slip at depth is accommodated at the surface by folding.

2. If S_{fault} (at depth) $>> S_{fold}$ (at the surface), the wrinkle ridge overlies a surface-breaking thrust fault, with folding primarily due to horizontal translation of the thrust sheet over the fault surface (e.g., Figure 2d). Given that $S_{fault} >> S_{fold}$ for the lunar examples investigated, *Golombek et al.* [1991] concluded that the thrust faults at depth likely reach the surface, implying to them that wrinkle ridge morphology is dominated by imbricate fault slices. They also inferred that the thrust fault cannot be "blind" and confined to depth because they thought that the shortening due to folding must then equal that due to fault slip. Their conclusion, combined with their application of the idea primarily to understand elevation offsets across wrinkle ridges, motivates the representation of their fault-based scenario as a single, surface-breaking fault, as shown in Fig-

ure 2b. Because fault slip and folding of the strata above are both parts of the same mechanical system [e.g., *Johnson and Fletcher*, 1994; *Cooke and Pollard*, 1997; *Roering et al.*, 1997; *Niño et al.*, 1998], however, the two components of horizontal shortening may not be added together to estimate a total horizontal shortening or strain across a wrinkle ridge. Nevertheless, the previous geometrically based hypotheses contained in the literature and discussed here present a qualitative basis for the present, mechanically based model discussed below.

5. Folding of Surface Strata

Balanced kinematic models for flexural slip folding above a thrust fault provide a means for evaluating wrinkle ridge shape in a semiquantitative way. This approach builds upon previous measurements of line length changes reconstructed across a wrinkle ridge at the planetary surface [*Golombek et al.*, 1991; *Watters and Robinson*, 1997] by using the simple geometry of published kinematic models of folding to extrapolate the deformation recorded at the surface to depth. Two classes of kinematic models potentially descriptive of planetary wrinkle ridges are called "fault-bend folds" (Figure 2d) and "fault-propagation folds" (Figure 2e) [e.g., *Suppe*, 1983; *Suppe and Medwedeff*, 1990; *Mitra*, 1990; *Chester et al.*, 1991; *Suppe and Connors*, 1992; *Mercier et al.*, 1997]. Fault-bend folds are formed as a geometric response of originally horizontal layers to flexure up and around geometric irregularities of the underlying fault surface (such as ramps that change dip angle in the slip direction of a thrust fault, when viewed in cross section). Fault-propagation folds are geometric models of displacement transfer from an underlying fault to overlying beds, resulting in folding above the fault tip.

Kinematic models typically are unable, by construction, to incorporate more than just the initial fault configuration [*Suppe and Medwedeff*, 1990; *Mitra*, 1990; *Chester et al.*, 1991] (but see *Mercier et al.* [1997] and *Shaw et al.* [1999] for methods to include additional forward breaking faults). This restriction means that the models would be most successful in reproducing the topography of wrinkle ridges that contained no other significant faults, such as splays [e.g., *Suppe and Connors*, 1992]. As noted by *Suppe and Narr* [1989], the growth of additional faults during fault-bend or fault-propagation folding could change the final fold morphology markedly from the initial kinematically based constructions. As a result, the topographic profiles of wrinkle ridges chosen should correspond to examples that lack well-developed wrinkles (possible splay faults) along their margins that would complicate or obscure the associated fold shape.

Geiser [1988] evaluated methods for constructing balanced cross sections of blind thrust faults and the associated folded strata. He emphasized that differences in the amount of horizontal shortening accommodated at the fault and above the blind fault tip may lead to "kinematically inadmissible" (i.e., unphysical) reconstructions if standard methods of area balancing and bed thickness of layers are rigidly enforced. This problem arises because the amount of shortening accommodated by folding differs from (and is usually less than) that due to faulting in these models. Further, area-balancing techniques that do not include layer-parallel shortening, layer thickness variations above the thrust [*Geiser*, 1988], and reductions in fault slip near fault terminations, produce unphysical reconstructions that poorly match subsurface data [*Mitra and Mount*, 1998]. These results imply that the strain compatibility relationships between near-surface anticlines and underlying blind thrust faults may not be adequately simulated using purely kinematic models and that predictions of shortening magnitudes obtained from these models may be subject to considerable uncertainty, depending on the level of sophistication of the model and the degree of field and subsurface control of the geologic structure (see discussions by *Stone* [1999] and *Mitra and Mount* [1999]). Nevertheless, the kinematic models of fault-bend and fault-propagation folds provide a useful starting point, but not the complete answer, for relating folding at the surface to faulting at depth.

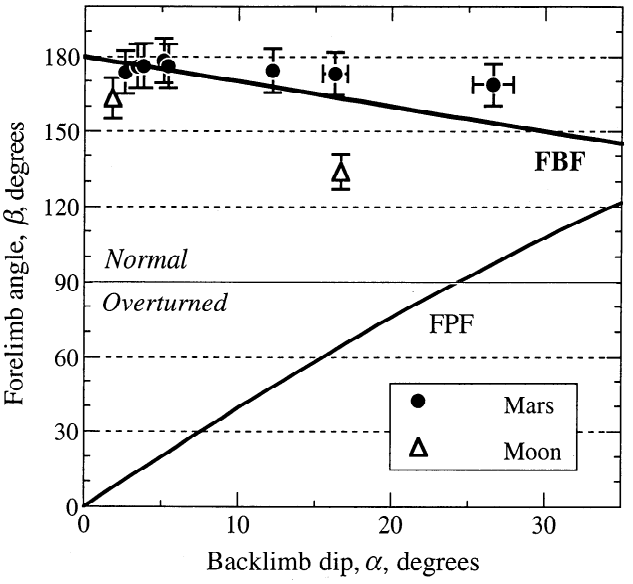

Figure 3. Test of kinematic fault-bend and fault-propagation folding models [*Mercier et al.*, 1997] using wrinkle ridge topography; parameters as in Figures 2d and 2e. FPF denotes fault-propagation fold; FBF denotes fault-bend fold. Uncertainties estimated from profiles measured by *Golombek et al.* [1991] and *Watters and Robinson* [1997].

The marginal slopes of several planetary wrinkle ridges, extracted from topographic profiles prepared by *Golombek et al.* [1991] for the Moon and by *Watters and Robinson* [1997] for Mars, were measured and compared to the predictions of these models. Of course, with no subsurface data available for particular wrinkle ridges, only the surface profiles and simplest kinematic models were used. Topographic profiles were chosen here for traverses across the simplest portions of the wrinkle ridges, as discussed above, and were obtained by *Golombek et al.* [1991] from available topographic maps and by *Watters and Robinson* [1997] from photoclinometry. The slope angles of the opposing edges (the trailing backlimb, α, and the leading forelimb, β, in Figures 2d and 2e) of several representative lunar and Martian wrinkle ridges were measured here and compared by using the method of *Mercier et al.* [1997]. The results (Figure 3) suggest that a fault-bend fold model is consistent with wrinkle ridge shapes at the planetary surface. Fundamentally, this result implies that flexure of a stack of multilayers can produce geometries consistent with wrinkle ridge topographies and supports the interpretation of wrinkle ridges as folds in near-surface rocks. This result appears to be general for morphologically comparable wrinkle ridges on other bodies, such as Mercury and Venus, for which analogous high-resolution topographic data are not yet available [*Kreslavsky and Basilevsky*, 1998; *Watters et al.*, 1998].

These geometrically simple kinematic folding models require, by construction, that fold geometry remain constant with depth

[e.g., *Woodcock and Fischer*, 1986]. However, decreases in fold intensity with distance from the subjacent fault are clearly demonstrated in natural examples and accurately simulated by using appropriate mechanical models that incorporate strain compatibility [e.g., *Suppe and Narr*, 1989; *Taboada et al.*, 1993; *Johnson and Fletcher*, 1994, pp. 387–388; *Cooke and Pollard*, 1997; *Fletcher and Pollard*, 1999]. This limitation is not significant for common applications such as imbricate thrust sheets [e.g., *Geiser*, 1988; *Suppe and Medwedeff*, 1990; *Mitra*, 1990; *Suppe and Connors*, 1992] in which the kinematically modeled folding is contained within a larger deforming matrix (e.g., duplexes and horses), leading to approximately homogeneous displacement conditions within the sheet. Inhomogeneous stresses such as those associated with fault terminations, however, typically produce structures (cracks, faults, folds) whose intensity and displacement magnitudes decrease with distance from the fault [e.g., *Rispoli*, 1981; *Ruegg et al.*, 1982; *Willemse and Pollard*, 1998]. Thus, although the fold profile of a wrinkle ridge at the planetary surface may be consistent with a kinematic fault-bend fold geometry, continuation of this same geometry to depths closer to a subjacent fault tip is neither required nor physically plausible for a blind fault-fold system.

Suppe and Connors [1992] demonstrated that the box-like morphology of ridges in the outer annulus of Artemis Corona on Venus was most consistent with fault-bend folding due to translation of crustal strata along a décollement and up over a ramp. A systematic decrease in relief toward the ridge termination, without an associated decrease in planimetric ridge width, was cited as definitive evidence for folding due to a ramp-and-flat geometry that soles into a basal décollement having constant depth beneath the ridge. The Artemis ridges show this type of termination, suggesting a fault-bend-fold geometry [*Suppe and Connors*, 1992]. The style of fold-and-thrust deformation documented by *Suppe and Connors* [1992] and *Williams et al.* [1994] for accretionary wedges on Venus (e.g., Artemis Chasma) differs substantially from that observed for ridged plains units and wrinkle ridges on that planet [e.g., *Bilotti and Suppe*, 1999]. Further, active regional-scale décollements on Earth and Venus require special conditions of elevated pore fluid pressure, rheology, or temperature [*Williams et al.*, 1994] that appear unlikely to be developed for typical wrinkle ridge occurrences on Mercury or the Moon. Comparison of the morphologies of the Artemis ridges with wrinkle ridges (e.g., the Martian example in Figure 1c) suggests that wrinkle ridges are not simple fault-bend folds above a ramp-and-flat fault configuration, given that both width and relief of wrinkle ridges can be observed to change systematically toward their terminations (e.g., Figure 1c).

Neither of the kinematic models (fault-bend fold or fault-propagation fold) can produce an explicit splay or backthrust (antithetic) fault as implied by the observations [e.g., *Howard and Muehlberger*, 1973; *Sharpton and Head*, 1988; *Golombek et al.*, 1991; *Mangold et al.*, 1998] or, interestingly, a regional elevation offset [*Golombek et al.*, 1989, 1991; *Golombek and Banerdt*, 1999; *Golombek et al.*, 1999, 2000] across the wrinkle ridge. Thus, while particular fold geometries at the surface may be adequately simulated by using a kinematic fault-bend-fold model, additional processes are required to fully account for the observed suite of wrinkle ridge characteristics. In particular, a physically based mechanism to produce splay faults and echelon wrinkle arrays during fault-related folding is required. Additionally, decreases in wrinkle ridge width and height along-strike, toward the ridge terminations (Figure 1c) and the suspected presence of differential vertical elevation offsets across wrinkle ridges [*Golombek et al.*, 1991; *Golombek and Banerdt*, 1999; *Golombek et al.*, 1999, 2000] both argue convincingly against a basal décollement [e.g., *Allemand and Thomas*, 1992; *Mangold et al.*, 1998] beneath wrinkle ridge terranes.

6. Blind Thrusts, Slip Localization, and Nucleation of Backthrust Faults

Field investigations and mechanical modeling of blind thrust faults associated with representative earthquake ruptures (e.g., 1980 El Asnam, Algeria; 1983 Coalinga, California; 1987 Whittier Narrows, southern California; 1994 Northridge, southern California) demonstrate that folding of near-surface strata, located between the blind thrust fault tip and the surface, is a fundamental and widespread process related to subsurface thrust faulting on the Earth [e.g., *Philip and Meghraoui*, 1983; *King and Yielding*, 1984; *Stein and King*, 1984; *Lin and Stein*, 1989; *Taboada et al.*, 1993; *Roering et al.*, 1997]. Thrust faults in layered strata may not break through to the surface, but instead can be "trapped" at shallow depth as blind faults [*Roering et al.*, 1997] by nucleating flexural slip along superjacent strata [*Cooke and Pollard*, 1997]. Flexural-slip anticlines, located above the upper thrust fault tip, grow there as a result of displacement accumulation along the subjacent fault.

Thrust faults are characteristically segmented and discontinuous in both the along-strike and downdip directions [e.g., *Aydin*, 1988; *Davison*, 1994], giving rise to a diverse assemblage of map view patterns. Thrust faults may be associated with sets of smaller, echelon thrusts oriented either parallel or antithetic to the main thrust fault and that may also display small components of strike-slip displacement [e.g., *King and Yielding*, 1984]. Systematic, localized rotations of the stress tensor about *xyz* axes are well known near the periphery of dip-slip faults in three dimensions [e.g., *King and Yielding*, 1984; *Crider and Pollard*, 1998], leading to echelon segmentation and a locally consistent sense of step of antithetic (backthrust) fault segments.

Numerical modeling of thrust-related deformation reveals the importance of layer characteristics (stratification and strain localization) and fault geometry in the resulting suite of near-surface structures. For example, calculations by *Cooke and Pollard* [1997] and *Roering et al.* [1997] demonstrate clearly that frictional slip along a blind thrust fault can nucleate slip patches [e.g., *Martel and Pollard*, 1989] along portions of superjacent bedding interfaces, promoting localized bedding plane slip and the growth of flexural slip folds in these layers above the fault. Because stress perturbations associated with fault slip in surrounding rock are greatest near the fault and decrease with distance from it, fold amplitudes decrease toward the surface, leading to gentle folds nearer the surface and tighter folds at depth near the fault [*Cooke and Pollard*, 1997]. Folding may not reach the surface if the fault is sufficiently deep. Although regional, far-field stresses associated with the thrust faulting may also promote layer-parallel shortening and folding of layers above, displacement along the fault facilitates folding by adding appropriate stresses and by localizing the flexure above it [e.g., *Roering et al.*, 1997].

The work of *Niño et al.* [1998] provides a compelling physical basis for relating near-surface folding to faulting at depth. Finite element calculations by *Niño et al.* [1998], carried out to large finite strains, confirm that moderate to low fault dips ($< 45°$), small interbed shear strength, and multiple layers promote folding above a blind fault. In contrast, a massively bedded sequence, or one with strong bedding planes, above a blind thrust fault tends to inhibit folding and promote upward propagation of the fault to the surface [*Roering et al.*, 1997], leading to a surface-breaking thrust fault [*Niño et al.*, 1998]. These published calculations motivate a physi-

cal explanation, developed below, for the wrinkle ridge-lobate scarp transition noted in the literature where the same structure (the blind thrust fault) crosses into different geologic units [*Lucchitta*, 1976; *Watters*, 1988, 1993; *Mangold et al.*, 1998].

Surficial folds can also be produced in poorly layered units such as soils due to fault-related displacements below [e.g., *Philip et al.*, 1992]. Several examples cited by *Plescia and Golombek* [1986], such as the Meckering, Australia anticline array, imply an association of wrinkle-ridge-like morphologies with soft sediment deformation. However, folding of material above blind thrust faults does not promote trapping of the fault tip at depth unless localized bedding plane slip [*Roering et al.*, 1997] is also a factor [*Niño et al.*, 1998]. Indeed, thrust faulting at Meckering typically broke through to the surface despite the existence of the folds [e.g., *Plescia and Golombek*, 1986]. The Meckering scarp may thus better serve as an example of a lobate scarp rather than a wrinkle ridge. Flexural slip folding of multilayers also produces kink-fold morphologies [*Suppe*, 1983] as long as bedding plane slip is localized [*Johnson and Fletcher*, 1994, pp. 345–347], instead of more rounded, sinusoidal fold shapes associated with freely slipping bedding planes [*Johnson and Fletcher*, 1994, p. 347] or continuum flow (see *Price and Cosgrove* [1990, pp. 241–272] for review of fold models and morphologies). We expect that the morphology of blind thrust anticlines on terrestrial planets should differ significantly , and systematically, for layered and nonlayered sequences, with surface-breaking faults being more common in poorly layered sequences (i.e., those with either massive bedding or strong, bonded interfaces).

Whereas typical fold-and-thrust belts may be characterized by forward breaking thrust faults along ramp-and-flat systems appropriate to accretionary (Coulomb critical taper) wedges [e.g., *Suppe and Connors*, 1992; *Mitra and Sussman*, 1997; *Shaw et al.*, 1999], the importance of backthrusts above individual planar blind thrust faults is becoming increasingly recognized, particularly in areas of active or single-phase deformation outside of accretionary prisms [e.g., *Hill*, 1984; *Stein and King*, 1984]. *Niño et al.* [1998] demonstrated that strain softening and localization in the overlying strata promote the nucleation and growth of backthrust faults (Figures 1a, 1b, and 1c). Strain softening is the time- and strain-dependent reduction from macroscopic peak strength to residual strength, related to the localization, growth, and linkage of joint and fault arrays in the layer. Formation of backthrust faults is prevented if strain localization is not allowed, as demonstrated in the physical experiments by *Chester et al.* [1991]. These small, antithetic thrust faults initiate because of favorable stress states caused by the localized occurrences of bedding plane slip, and attendant flexural slip folding [*Cooke and Pollard*, 1997], above the blind fault. The newly formed backthrust faults will nucleate with small displacements and lengths appropriate to fault-scaling relationships [e.g., *Cowie and Scholz*, 1992; *Schultz*, 1997, 1999] and increase in size and displacement as they propagate toward the planetary surface. The resulting fault that eventually breaks the surface may inherit a complex, echelon configuration from the inhomogeneous stress state developed above the blind thrust fault.

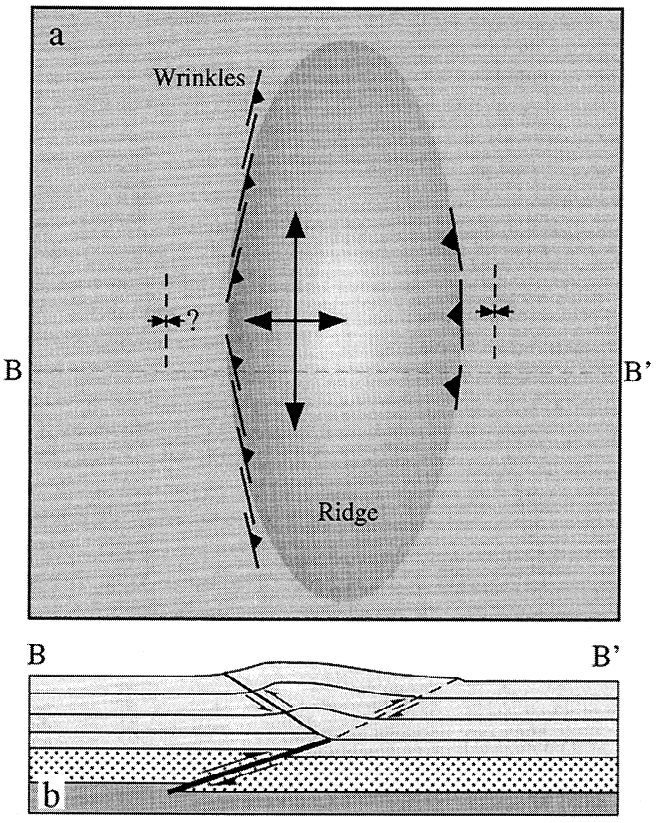

Figure 4. Synoptic blind thrust model for wrinkle ridges; overall direction of thrusting is left to right. (a) Structural map showing major elements of wrinkle ridge morphology; along-strike length is greatly reduced, relative to ridge width, in the figure. Section line B–B' shows position of cross section given in Figure 4b; surface breaks of thrust faults are shown with teeth on their particular upper plate; anticlines and potential synclines are shown by converging and diverging arrows, respectively. Upper plate of wrinkle ridge-blind thrust fault system includes the ridge and extends to its left. (b) Cross section showing blind thrust fault (heavy line showing thrust displacement) beneath flexural slip anticline, backthrust fault (putative wrinkle), and updip prolongation of main fault surface (dashed).

7. A New Synoptic Model for Wrinkle Ridges

The observations of wrinkle ridge morphology, combined with the recent results for folding above blind thrust faults discussed above and in the literature, motivate an integrated, mechanically based model for wrinkle ridge development (Figure 4). This new synoptic model, described in this section, incorporates the key elements discussed above and helps to resolve or clarify many of the ambiguous or controversial issues in wrinkle ridge tectonics, as listed in Table 1 and debated in the literature. It may also motivate a more coherent terminology. Although some previous faulting-based models for wrinkle ridges have invoked blind or surface-breaking thrust faults (e.g., Figures 2b, 2d, and 2e), those conceptual scenarios were unable to provide a physical basis for systematically relating the morphology and topography of wrinkle ridges to the postulated subsurface structure. This one does. The synoptic model laid out in this section is rooted in the mechanics of blind thrust faulting [e.g., *Cohen*, 1999], detailed field investigation of terrestrial blind thrust anticlines [e.g., *Philip and Meghraoui*, 1983; *King and Yielding*, 1984; *Stein and King*, 1984], and explicit numerical modeling of coupled fault-fold systems [e.g., *Cooke and Pollard*, 1997; *Roering et al.*, 1997; *Niño et al.*, 1998].

In the synoptic blind-thrust model developed here, the wrinkle ridge is the surface expression of an anticline formed by flexural slip folding of near-surface strata (Figure 4a). The anticline can be asymmetric, with the position and degree of asymmetry dependent on the details of folding, subsurface blind fault geometry, and the

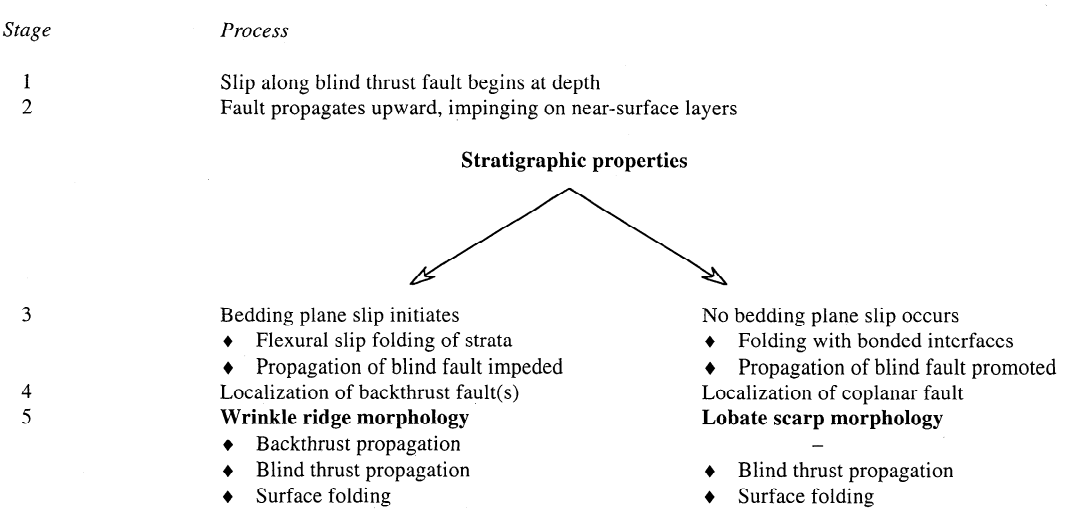

Figure 5. Deformation sequence for wrinkle ridge and lobate scarp formation based on the blind thrust model developed in this paper.

development of backthrusts. Wrinkles are formed as echelon arrays of small backthrust faults that nucleate at depth near the main blind fault and propagate up toward the surface. The sense of step of echelon wrinkles is related to local rotations in the three-dimensional (3-D) stress tensor above the blind fault edge, producing characteristic patterns at the surface (Figure 4a); these initial step senses may be modified or superseded by a regional stress state that is resolved across the ridge trend. Scarps that sometimes bound the margins of wrinkle ridges are the surface traces of backthrust faults or the main blind thrust fault that also has propagated to the surface during the growth and development of the anticline. As demonstrated below, a gentle syncline (perhaps without brittle fracturing for this low-strain area) could potentially develop behind the wrinkle ridge on the upper plate, for specific conditions of large displacement gradient at the lower fault tip; its location would be associated with that of the lower tip of the blind fault (Figures 4a and 4b). A tighter, yet still subtle, syncline can also grow adjacent to (and ahead of) the main thrust fault scarp after the blind fault has propagated to and broken the surface. This also leads to a steeper forelimb, with locally overturned strata at the location of the surface break, that may be well developed for lobate scarps but not significant (or even present) for wrinkle ridges. However, both the leading syncline and steep stratal dips in the vicinity of the surface break are commonly observed along terrestrial thrust faults [e.g., *Stein et al.*, 1988].

Wrinkle-ridge-like morphologies can be produced due to slip along blind thrust faults [*Niño et al.*, 1998] if layers above the upper fault tip slip along bedding and fold (Figure 4a) and if backthrust faults develop. The thickness of the folding section corresponds to the depth below the surface of the blind thrust fault's upper tip, rather than some specific stratigraphic thickness or basal décollement. As displacement builds up on the blind thrust fault (Figure 5), folding of overlying strata begins and triggers growth of the backthrust fault array for particular conditions (Figures 1a and 4b). At a late stage in the deformation, the blind thrust fault may begin to propagate upward toward the surface [*Niño et al.*, 1998]. The resulting assemblage of structures (blind thrust fault, overlying flexural slip fold, and antithetic backthrust faults) creates the basic wrinkle ridge morphology.

The specific sequence (and surface morphology) depends on the interplay between displacement accumulation along the main blind thrust fault; the rate, mechanisms, and geometry of folding; and the efficacy of strain localization in the deforming sequence. As a result, a variety of wrinkle ridge morphologies is possible. For example, the pattern and location of wrinkles may vary along the wrinkle ridge depending on the specific geometry of the folding sequence (e.g., variations in layer thickness or interface strength along-strike). The dip direction of the wrinkle-forming backthrust faults, the parent blind thrust fault, or both, may change along-strike depending on the associated stress state, leading to reverses in elevation offset, ridge asymmetry, and wrinkle location at the surface. Detailed mapping is required to systematically relate specific geologic environments to wrinkle ridge morphology beyond the broad template outlined above. In addition, the seismic potential of wrinkle ridges [*Golombek et al.*, 1992] will likely require upward revision by analogy with terrestrial blind thrust faults and attendant coseismic folding [e.g., *Hill*, 1984; *Stein and King*, 1984; *Lin and Stein*, 1989; *Taboada et al.*, 1993; *Shaw and Suppe*, 1996] if some of the Martian structures are still active.

7.1. The Strain Problem: Faulting or Folding?

The quantitative inversion of wrinkle ridges for strain, both for the planetary surface and at depth, has been a long-standing and critical problem [e.g., *Golombek et al.*, 1991; *Watters and Robinson*, 1997]. The uncertainty in assigning strain magnitudes to wrinkle ridges stems mostly from disagreements on the physical basis for interpreting the contractional strains (e.g., folding versus faulting models; see *Golombek et al.* [2000], *Montési et al.* [2000], and *Watters and Robinson* [2000] for recent approaches). The blind thrust model developed in this paper helps to clarify the relationship between surface and subsurface strains.

The surface strain represented by a wrinkle ridge anticline is not simply related to that at depth along the fault, as assumed in many kinematic models of folding and some previous studies of wrinkle ridges, given that the amount of strain at the surface is modulated by the thickness of strata above the fault tip and their flexural slip offsets. This coupling between potential folding at the surface and faulting at depth is explored here by calculating the amounts of horizontal shortening at both levels.

7.1.1. Approach. In this and the following sections, a standard mechanical model is used to calculate the stresses and displace-

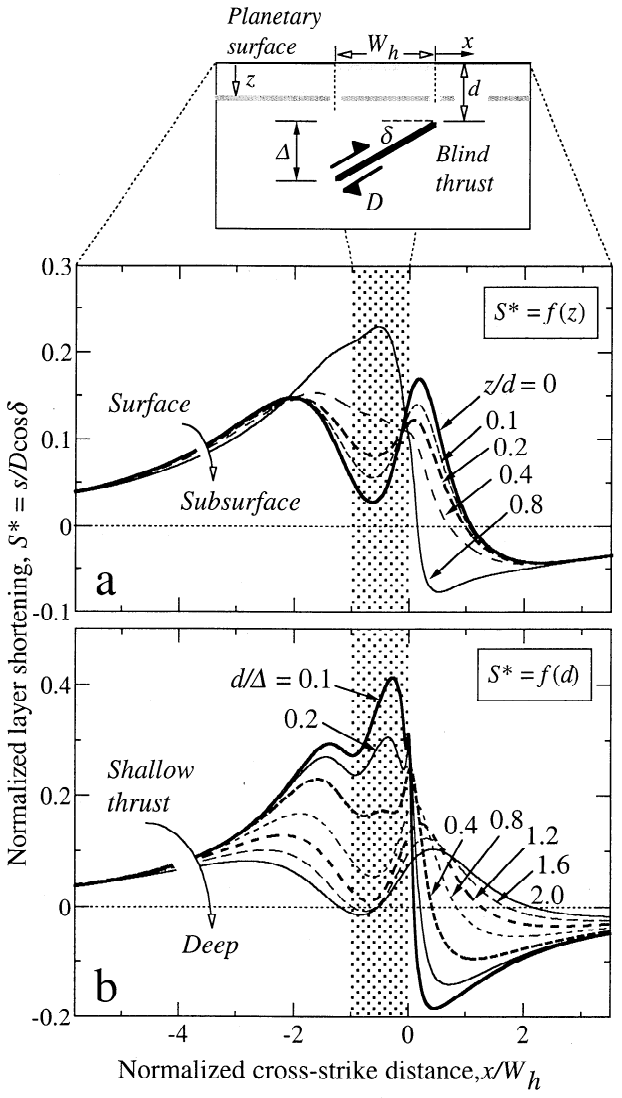

Figure 6. Horizontal shortening of planetary surface (normalized to fault throw $D\cos\delta$) depends on position, x, relative to blind fault (normalized to horizontal extent of subsurface fault, W_h, shaded). Profiles calculated using fault dip $\delta = 30°$, thrust offset D = 10 m, and depth extent of faulting Δ = 5 km, measured from upper fault tip (d = 5 km) to lower tip depth (10 km). (a) Normalized horizontal shortening of layers at various depths beneath the surface. The upper fault tip is located at z/d = 1.0. (b) Normalized horizontal shortening of the planetary surface for range of blind fault depths.

ments induced by slip along a blind thrust fault. For simplicity we do not explicitly model either bedding plane slip or backthrust fault nucleation and growth, in part because these two processes are adequately documented in the literature (see *Cooke and Pollard* [1997], *Roering et al.* [1997], and *Niño et al.* [1998] for representative and explicit treatments). However, the model used here provides predictions of initial stress changes and displacements (associated with initial, putative folds) that are fully consistent with the simulations of particular scenarios run out to much larger strains and published by *Niño et al.* [1998] and others. The basic mechanical model used here demonstrates key principles that apply regardless of the magnitude of either backthrust faulting or surficial folding, and points the way toward more comprehensive mechanical modeling of wrinkle ridges once their morphologies and topographies have been more systematically documented.

Horizontal displacements are calculated here for rocks above an initial blind thrust fault (assuming no bedding-parallel slip), using the 3-D boundary element program COULOMB [*Toda et al.*, 1998], which uses the stress functions derived by *Okada* [1992]. In this formulation, slip is prescribed along the blind fault, which has a specified geometry and position in an elastic half-space; the slip induces displacements and stress changes in the material above [e.g., *Bruhn and Schultz*, 1996; *Crouch and Starfield*, 1983]. In this dislocation-type approach, any far-field stresses or remote tectonic contraction would be added to the solution once they are known, resulting in stress and displacement fields somewhat different in detail, but not in character, than those presented in this paper. The elastic half-space solution is an appropriate first step to modeling the initial response of rock or layers to fault-induced displacements (e.g., see *Taboada et al.* [1993] and *Cohen* [1999]); future work (in progress) that incorporates more general rheologies, stratification, and strain localization explicitly can then be related to specific examples of wrinkle ridge morphology and topography.

A range of parameters was investigated. In the example considered here, the blind thrust fault is located at $5 \le d \le 10$ km below the surface, with a strike-parallel length of L = 40 km, a vertical extent of $\Delta = (10–5) = 5$ km, a downdip fault width of $w = \Delta(\sin\delta)^{-1} = 10$ km, and a dip of $\delta = 30°$ (Figure 6, inset). These parameters permit an eventual backthrust fault to nucleate at the blind fault's upper tip and to propagate to the surface in the vicinity of the opposite (trailing) side of the ridge anticline. A reverse (thrust) displacement of D = 10 m was applied across the fault, producing a horizontal fault throw (the "shortening due to faulting") of $S_{fault} = D\cos\delta = 8.66$ m. Displacements of material points elsewhere in the surrounding rock mass, discussed below, are normalized by the values of fault size (L, and cross-strike extent in map view (vertical projection of downdip width), $W_h = \Delta(\tan\delta)^{-1} = 8.66$ km), position beneath the surface (d = 5 km), and horizontal throw (S_{fault}) to facilitate comparisons between the various parameters. Properties of the faulted half-space appropriate for the near-surface region [*Schultz*, 1996] are given by deformation modulus E^* = 1 GPa and Poisson's ratio $\nu = 0.25$. Fault slip that is related explicitly to remote stresses and constitutive properties of the fault zone (e.g., frictional resistance) would produce results comparable to those shown here. Although the details of stress or displacement magnitudes would change with other choices of plate and fault properties, the overall conclusions of this study are generally insensitive to the particular values used. This means that subtle features in the stress or displacement fields should not be related too strenuously to particular features in either images or topographic profiles of actual wrinkle ridges, but the overall characteristics may be relevant as a guide to a variety of wrinkle ridge occurrences.

7.1.2. Displacements of particular horizons. Calculations of the predicted horizontal shortening displacements are shown in Figure 6 for ridge-normal transects located at various depths below the surface (and above the fault). In the calculations the horizontal shortening s for each point along the flat horizon at the given depth is normalized by the horizontal component of displacement (the initially specified throw across the fault) accommodated by the dipping fault (S_{fault}; see above text and inset to Figure 6 for parameters) to produce a normalized layer shortening $S^* = s/S_{fault}$. The horizontal position, x, relative to the surface projection of the blind fault (inset, stippled in Figures 6a and 6b) is normalized by the fault extent W_h. Horizontal shortening is the component of displacement parallel to the fault throw and normal to the fault strike.

Two cases illustrated in Figure 6 show traverses constructed normal to the fault, and through its midpoint, for various horizons.

In the first case (Figure 6a), normalized horizontal shortening of layers located at various depths beneath the surface (and above the thrust) demonstrates that horizontal shortening and normal strains are fundamentally depth dependent. For example, the amount of shortening above the fault is greatest at depths just above the blind fault tip (i.e., $z/d > 0.8$) and rapidly decreases vertically with distance above the fault to minimum values at the surface ($z/d = 0$). In this example, the horizontal shortening above the fault (at the planetary surface) is <20% of the horizontal component of fault slip at depth (the curve for $z/d = 1.0$, not shown, would peak at values of $S^* = \pm 0.5$ at the fault). Note that "unrolled" profiles of wrinkle ridges span the part of the curve emphasized here, for $-0.5 < x/W_h < 1$. The results demonstrate that measurements of surface shortening and normal strain, estimated by "unrolling" the surface anticlinal topography [e.g., *Watters*, 1988; *Golombek et al.*, 1991; *Watters and Robinson*, 1997], cannot be related alone to the fault offsets or used as a definitive test of folding-based or faulting-based models for wrinkle ridge development.

In Figure 6b the normalized horizontal shortening of the planetary surface is calculated for a range of blind fault depths. In all cases considered here, the fault spans a constant depth interval $\Delta =$ 5 km between its upper and lower tips (inset, Figure 6). The results demonstrate that the horizontal shortening across a wrinkle ridge, measured at the surface, depends critically on how deep the blind thrust fault is below the surface. For example, moving the blind fault vertically down from a shallow depth $d = 500$ m ($d/\Delta = 0.1$ in Figure 6b) to a large depth of $d = 10$ km ($d/\Delta = 2.0$) leads to a reduction of horizontal shortening of the surface, from 40% of the shallow fault's throw to less than 10% for that of the deep fault (recall that the throw of both faults is held constant). As a result, the ratio of surface shortening to fault throw can be difficult to interpret without explicitly considering the depth of the blind fault.

The calculations shown in Figure 6 demonstrate that while the shortening and strain are maximized along the buried fault, the overlying rocks are shortened progressively less with increasing distance above the fault. As a result, the planetary surface can exhibit a mappable shortening significantly less than that at depth. The ratio of folding to faulting strains for wrinkle ridges is thus strongly dependent on the depth of the blind thrust fault below the surface, although the ratio for particular wrinkle ridges may also be modulated by the amount of regional contraction associated with fault-related shortening. These calculations provide the physical basis for the inference that faulting strains typically exceed those due to surface folding [*Golombek et al.*, 1991; *Watters*, 1991] yet clearly demonstrate the fundamental fault depth dependence of wrinkle ridge strain.

7.1.3. Displacements at the surface. Deformation of the planetary surface above a blind thrust fault produces a spatially varying, inhomogeneous displacement field [e.g., *Mansinha and Smylie*, 1971; *Ma and Kusznir*, 1992, 1993; *Taboada et al.*, 1993; *Cohen*, 1999]. The predicted deformation above a 3-D blind thrust fault is calculated for the planetary surface and shown in Figure 7. The predicted patterns of horizontal shortening (contraction and extension) and vertical displacement (uplift and subsidence) are comparable to those reported in previous models of terrestrial blind thrust faults. The effect of changing the fault shape to elliptical (rather than rectangular as used here) and using a slip gradient along the fault (rather than a constant value of fault offset) is a small reduction in the along-strike spread of the contours and a reduction in the displacement magnitudes [*Ma and Kusznir*, 1992]. However, these hypothetical variations do not significantly alter the conclu-

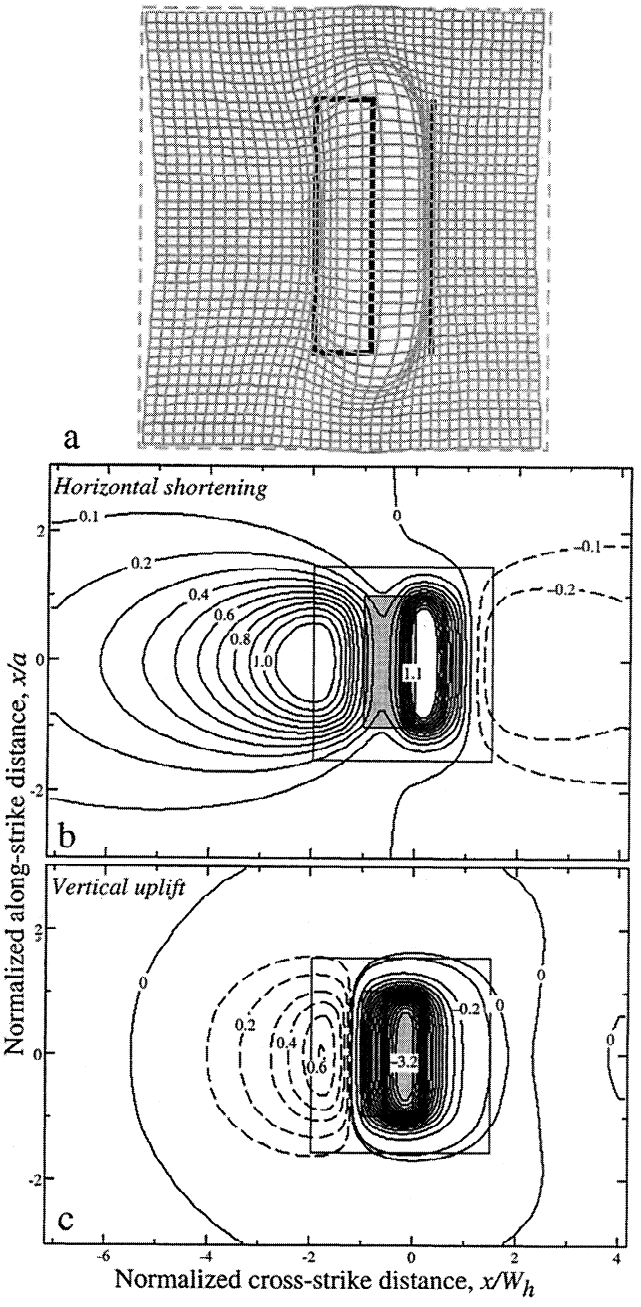

Figure 7. Deformation fields at the surface associated with slip along blind thrust fault. Thrust direction (vergence) is to the right. (a) Deformed grid in map view, constructed from both vertical and horizontal displacements of surface rocks. Inner box shows projected surface trace of blind thrust fault, dipping 30° down to the left (see inset, Figure 6); dashed line shows projected surface break above upper fault tip. Outer dashed box shows the undeformed area; deformed grid includes both vertical and horizontal components of displacement. (b) Horizontal shortening, in meters, calculated for the planetary surface above a 3-D blind thrust fault having length $L = 2a = 40$ km. Dashed contours denote local small-strain extension ahead of thrust. Box shows location of grid in Figure 7a; smaller shaded box shows areal extent of blind fault plane (width, $-1 \le x/a \le 1$; normalized cross-strike distance, $-1 \le x/W_h \le 0$). (c) Vertical uplift, in meters, calculated for the surface above blind thrust fault; dashed contours show subsidence in potential trailing syncline on upper plate of thrust.

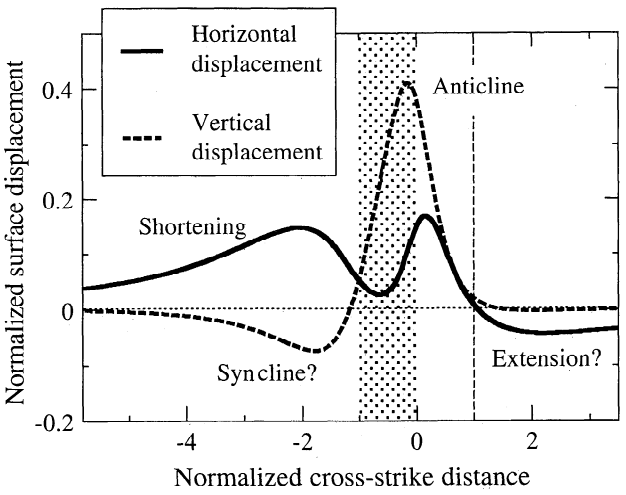

Figure 8. Comparison of horizontal and vertical displacements of the planetary surface above a blind thrust fault. Both values are normalized by the horizontal fault throw at depth, S_{fault}. Shaded area shows projected mapview extent of blind fault plane; dashed vertical line shows updip projection of blind fault and location of potential surface break. Horizontal shortening (solid curve) occurs for positive values behind the potential surface break; minor extension is predicted ahead of the break. Vertical uplift (dashed curve) occurs over the blind fault to the projected surface break; a gentle trailing syncline may develop behind the fault at the surface in the upper plate.

sions presented in this section given that the associated changes are minor relative to the nature and shape of the displacement patterns themselves.

The deformed grid, obtained by calculating the map view displacement vectors (horizontal and vertical) and rendering them as synthetic topography (Figure 7a), illustrates graphically that surface rocks in map view are squeezed or stretched depending on their position relative to the underlying fault. Calculations of horizontal shortening, in map view, show that most of the deformation occurs behind the surface projection (line in Figure 7a) of the blind fault plane (i.e., above the thrust), with some shortening also produced well behind the position of the lower fault tip on the upper plate (left-hand edge of deformed grid in Figure 7a). This implies that deformation of surface rocks (second-order folding, reverse faulting, jointing) in the areas between wrinkle ridges may be produced in association with slip along the main fault beneath a particular ridge. A subtle region of potential low-strain horizontal extension is also implied for the area within perhaps five fault widths ahead of the wrinkle ridge (Figure 7a, dashed contours).

Horizontal and vertical displacements at the planetary surface, due to slip along the blind thrust fault at depth, are compared in Figure 8. Both values are normalized to the "shortening due to faulting," S_{fault}. The wrinkle ridge anticline is predicted to occur for $-1 < x/W_h < 1$, or over the area of the fault plane and extending forward to the point of projected surface break (dashed vertical line in Figure 8). The amount of normalized uplift exceeds the normalized shortening by about a factor of 2 in the future ridge area. Interestingly, a subtle syncline may develop behind the ridge, extending back perhaps four ridge widths at the surface, but only if the lower fault tip is unbounded (i.e., does not end within ductile or viscoelastic material) and characterized by a steep displacement gradient [e.g., *Taboada et al.*, 1993]. The presence or absence of such synclines behind actual wrinkle ridges may be indicative of the character of fault terminations at depth.

Horizontal shortening occurs at the surface from the projected surface break back, on the upper plate, for at least seven ridge widths (Figure 8, solid curve). Horizontal shortening of at least 10% of the fault throw occurs for distances of approximately three fault widths behind the ridge. These profiles reveal that wrinkle ridge deformation may extend over broader areas than just the ridge itself. The spatial extent and pattern of surface deformation discussed here may be modified, however, by the development of echelon backthrust faults (wrinkles) and by flexural slip folding of the near-surface strata [e.g., *Niño et al.*, 1998]. As a result, the predicted spatial scales noted here for the simplest cases may require some modification for comparison with particular examples of actual wrinkle ridges.

The results presented in Figures 6–8 demonstrate that the horizontal shortening associated with slip along a blind thrust fault is spatially inhomogeneous in three dimensions, in that it varies with position relative to the fault in both the vertical and horizontal directions. Estimates of surface shortening in the vicinity of a wrinkle ridge are thus dependent on their position (both along-strike and cross-strike) relative to the ridge, as well as on the depth to the blind thrust fault. These calculations also demonstrate that wrinkle ridge deformation may extend to large areas between the ridges. For a fault depth and wrinkle ridge width of 10 km, rocks at the surface and in the subsurface are likely perturbed to perhaps 50 km or more on either side of the wrinkle ridge. We expect that wrinkle ridges that are relatively closely spaced (i.e., <50 km for the examples considered) may not develop in isolation but as part of an interacting system or population of wrinkle ridges.

7.2. Blind Thrust Faults and Topographic Offsets

The presence or absence of a vertical topographic (elevation) offset across a wrinkle ridge has been suggested to be diagnostic of faulting- or folding-based models [e.g., *Golombek and Banerdt*, 1999; *Golombek et al.*, 1991, 1999, 2000]. Significant offsets are not predicted by standard buckling models that assume layer-parallel compression of the lithologic sequence [e.g., *Watters*, 1991] unless shear strain within folds is significant. On the other hand, simple kinematic models of faulted layers [e.g., *Golombek et al.*, 1991; *Plescia*, 1991, 1993] have been used to suggest a characteristic vertical topographic offset, higher on the upper (rigid) plate, having magnitude $h = s \tan\delta$, where δ is the fault dip angle and s is the shortening across the fault at depth below the ridge (Figure 2b).

The origin, spatial distribution, and time dependence of vertical displacements (uplift and subsidence) at the surface related to slip along blind thrust faults are well known [e.g., *Savage and Hastie*, 1966; *Mansinha and Smylie*, 1971; *Rundle*, 1982; *Cohen*, 1984, 1999; *Li*, 1987; *King et al.*, 1988; *Stein et al.*, 1988; *Ma and Kusznir*, 1992; *Cooke and Pollard*, 1997]. Coseismic slip along a fault induces uplift of the surface above the fault plane and a small amount of subsidence both ahead of and behind the anticline [*Cohen*, 1984; *Ma and Kusznir*, 1992; *Taboada et al.*, 1993; *Freed and Lin*, 1998] (see Figures 7a and 7c). In addition, however, postseismic deformation of the surface typically occurs over longer timescales when the faulted brittle/elastic layer overlies a viscous or viscoelastic channel such as ductile lower crust [*Rundle*, 1982; *Cohen*, 1984; *King et al.*, 1988; *Freed and Lin*, 1998]. *Melosh* [1983] and *Cohen* [1984] have demonstrated that additional postseismic uplift of the coseismically produced anticline over a fault will occur if the depth of faulting is greater than about 70% of

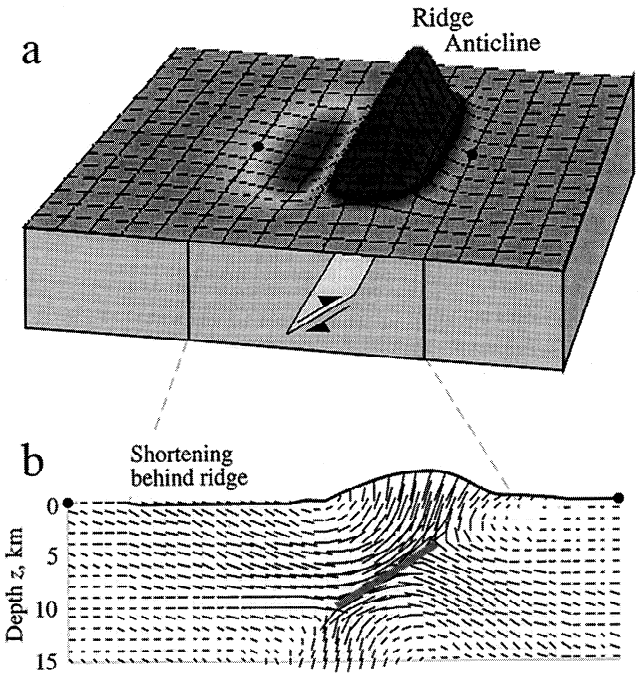

Figure 9. (a) Representative vertical displacements of the surface due to slip on blind thrust fault; parameters as given for Figures 6 and 7. Uplifted topography is produced above the position of the blind fault in the subsurface. (b) Displacement vectors for a section through the ridge midpoint showing interplay between the vertical and horizontal components. Horizontal shortening behind the ridge (see Figure 7b) is indicated.

the thickness of the brittle layer. Postseismic subsidence can potentially occur in that area over smaller faults. *Freed and Lin* [1998] demonstrated that postseismic stress relaxation in subjacent viscous crust can augment surface elevations behind the fault plane. Although the additional topography associated with such stress relaxation may be difficult to distinguish from postseismic afterslip on the blind fault without precise geodetic leveling data covering a sufficiently long time period, both sources of postseismic elevation change may contribute to the final surface topography [*Freed and Lin*, 1998].

The predicted pattern of vertical displacements calculated for the ground surface above a bounded blind thrust fault is shown in Figure 7c. The contours show areas of predicted coseismic uplift and subsidence (dashed contours behind the thrust) that appear to correlate with the overall topography of wrinkle ridges (Figure 1). Although temporal data are unavailable for Martian wrinkle ridges, the vertical displacement pattern shown in Figures 7c, 8, and 9 should approximate the first-order topography above both lobate scarps (which lack flexural slip folding and significant backthrust faults) and perhaps wrinkle ridges, with potential contributions from postseismic relaxation below the fault being of secondary importance [e.g., *Freed and Lin*, 1998]. Of course, flexural slip folding and accumulation of displacements along backthrust faults (wrinkles; not explicitly modeled in this study) should also modify this initial topography, leading to differences in ridge asymmetry, amplitude, and wavelength for particular cases [e.g., *Niño et al.*, 1998].

Significant vertical displacements of surface rocks are associated with blind thrust faults (see Figures 7b and 8). Uplift occurs above, and ahead of, the fault surface (Figure 9; see also *Taboada et al.* [1993], *Cooke and Pollard* [1997] and *Freed and Lin* [1998] for comparable results). The uplift is principally developed within the horizontal region bounded by the surface projection of the upper fault tip (dashed line in Figure 8) and the vertical projection of the lower fault tip. This region spans a distance of two fault widths, or one ridge width ahead of the ridge (~10 km) in the examples considered here. Displacement vectors in the subsurface (Figure 9b) demonstrate how uplift (or subsidence) and shortening are related at the surface and below. A subtle trailing syncline, if produced, may be predicted to extend approximately two fault widths, or ~20 km, behind the wrinkle ridge (Figures 8 and 9); this feature's existence depends critically on the details of displacement distribution along the blind thrust fault and may not be developed in actual cases. Topographic profiles that adequately represent the topography associated with wrinkle ridges developed over blind thrust faults must therefore span a distance greater than approximately two fault widths on either side of the ridge, or a total distance of at least 50 km for the present example. Shorter profiles may measure only an incomplete subset of the topography, potentially leading to erroneous conclusions about fault-related topography. These results support the conclusions of *Watters and Robinson* [1997] that the choice of baseline is important for definitively assessing wrinkle ridge topography.

7.3. Backthrust Faults and the Wrinkle Ridge—Lobate Scarp Transition

One area of significant difference between wrinkle ridges and lobate scarps is the surface expression of the underlying fault(s). Backthrust faults (wrinkles) are an essential and characteristic feature of wrinkle ridges, whereas these antithetic fault arrays are generally lacking in association with lobate scarps [e.g., *Watters*, 1993; *Watters and Robinson*, 1997]. On the other hand, surface breaks are documented ahead of both wrinkle ridges and lobate scarps but are more common or pronounced for lobate scarps. In this section I examine the tendency for blind thrust faults to propagate toward the surface by relating potential areas of fault localization to areas of predicted Coulomb stress change.

Slip along a fault changes the state of stress in its vicinity, and the magntiude and sense of these inhomogeneous stress perturbations vary with proximity and the relative position to the fault [e.g., *Chinnery*, 1963; *Rudnicki*, 1980; *Segall and Pollard*, 1980; *Li*, 1987; *Pollard and Segall*, 1987; *King et al.*, 1994]. Changes in stress state and displacement are greatest near the fault and decrease to negligibly small values at distances of perhaps two to three fault lengths away [e.g., *Chinnery*, 1961, 1963; *Segall and Pollard*, 1980; *Barnett et al.*, 1987; *Aydin*, 1988; *Ma and Kusznir*, 1993]. Fault slip leads to changes in the magnitudes of normal and shear stress (σ_n and τ, respectively) resolved on surfaces of given relative orientation. The "Coulomb failure stress" [e.g., *Harris and Simpson*, 1992; *Stein et al.*, 1992; *King et al.*, 1994; *Bruhn and Schultz*, 1996; *Harris*, 1998] explicitly compares the perturbed stress components to the Coulomb frictional sliding criterion $|\tau| = \mu\sigma_n$ (where μ is the coefficient of maximum static friction) to determine if fault slip can trigger or impede frictional sliding on the other surface.

Previous work has demonstrated that lobes of increased Coulomb failure stress develop within the surrounding rock mass in directions normal to the fault plane (the "antithetic lobes" of *Freed and Lin* [1998]) as well as parallel to the fault. These lobes of increased Coulomb stress are associated in nature with aftershock locations following large earthquakes [e.g., *Harris and Simpson*, 1992; *Stein et al.*, 1992, 1994; *King et al.*, 1994; *Perfettini et al.*, 1999], suggesting that these lobe-like areas can influence regional

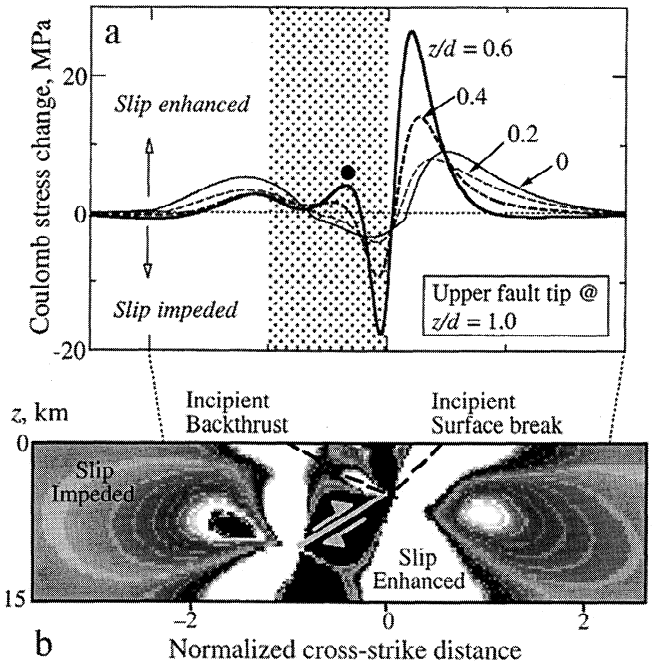

Figure 10. Changes in predicted Coulomb failure stress due to slip on blind thrust fault showing areas of enhanced fault slip and potential fault localization; parameters as given for Figures 6 and 7. (a) Profiles of predicted Coulomb stress change shown for various discrete depths, $3 \le z \le 0$ km (corresponding to $0.6 \le z/d \le 0$), from above the upper fault tip to the surface. Note significant enhancement of fault slip at depth in the antithetic (backthrust) region (solid circle). Horizontal extent of subsurface fault is shaded. (b) Distribution of predicted Coulomb stress changes in vertical section located across midpoint of blind fault, showing areas of enhanced and impeded slip along optimally oriented surfaces in rock surrounding the fault. Note lobe of enhanced slip at upper fault tip in area of future backthrust.

deformation surrounding the fault. Increased Coulomb stress promotes frictional sliding along favorably oriented surfaces, whereas decreased values can inhibit slip along these surfaces [e.g., *King et al.*, 1994; *Harris*, 1998]. *Freed and Lin* [1998] have evaluated postseismic changes in the crustal stress state associated with fault-induced ductile flow and stress relaxation in subjacent viscous lower crust or upper mantle. They found that Coulomb stress changes near the free surface above a blind thrust fault can increase in magnitude as this time-dependent stress relaxation proceeds, leading to an increased tendency for slip along antithetic backthrust faults above the main fault. The combined pattern of Coulomb stress change (coseismic plus interseismic) above the blind fault is qualitatively consistent with the calculations shown in Figure 10, suggesting that backthrust fault arrays should be a persistent attribute of wrinkle ridge growth.

Changes in predicted Coulomb failure stress are calculated here using COULOMB to examine the effect of slip on a blind thrust fault on near-surface rocks. The stress changes are calculated for each point in a grid (having a spacing of 0.1 km in each of the x, y, and z directions) surrounding the fault. The results are shown in Figure 10. Areas of enhanced fault slip for favorably oriented fracture surfaces (calculated by using a typical friction coefficient $\mu = 0.4$ [e.g., *Harris and Simpson*, 1992; *Stein et al.*, 1992; *King et al.*, 1994; *Sibson*, 1994; *Roering et al.*, 1997]) are unshaded, whereas areas in which slip is impeded are shown in darker shades. The calculations show Coulomb stress changes induced by slip along the blind thrust fault alone, in the absence of confining pressure or tectonic stresses, given that the total stress states associated with wrinkle ridge development on Mars are unknown. The addition of confining pressure and/or tectonic stresses would reduce or suppress slip enhancement to a greater degree at depth than at the surface. As a result, the stress changes for areas between the upper blind fault tip and the free surface are relatively unaffected by the choice of stress state.

The results shown in Figure 10 suggest that new thrust faults are favored to occur in either of two principal areas beneath the planetary surface: (1) updip of, and coplanar with, the blind fault plane, and (2) just above the fault's upper tip and antithetic to the fault plane. The magnitude of Coulomb stress change is initially greater in the first area (updip of the fault) than in the second one (antithetic to the first; large dot in Figure 10). In the first case the blind thrust fault would propagate to the surface to produce a lobate scarp with a clear surface break [*Niño et al.*, 1998]. However, the degree of Coulomb stress change in the second location can be sufficient to promote growth there of an antithetic backthrust fault (small lobe in Figure 10b), especially if the magnitude of stress change in the first area is reduced by a process such as flexural slip folding [e.g., *Cooke and Pollard*, 1997; *Roering et al.*, 1997]. *Niño et al.* [1998] demonstrated that triggering of bedding plane slip by the blind thrust fault can both impede the fault's upward propagation and promote the growth of the backthrust fault array (nucleating within the second, antithetic lobe of Coulomb stress change), eventually leading to surface morphologies analogous to wrinkle ridges. The calculations shown in Figure 10, along with the results reported by *Cooke and Pollard* [1997], *Roering et al.* [1997], and *Niño et al.* [1998], indicate that near-surface flexural slip folding is the key ingredient that determines mechanically whether a wrinkle ridge or a lobate scarp develops above a blind thrust fault (see Figure 5).

Widespread regions of inhibited slip are also developed at further distances from the blind fault, as shown in Figure 10b. Slip along potential thrust faults located approximately two fault widths beyond either side of the wrinkle ridge, and extending to the surface, would be inhibited by coseismic slip along the blind fault plane. Flexural slip folding beyond the ridge region would also be inhibited by the slip-induced stress changes. Using the blind thrust model as a guide, the characteristic spacing of wrinkle ridges noted in the literature [e.g., *Watters*, 1991] may be influenced by stress changes associated with coseismic slip and/or postseismic relaxation associated with blind faults beneath the ridges. If correct, the spacings should scale with blind thrust fault size and the slip magnitude along it.

Displacement along the blind thrust fault can lead to stress changes resolved on potential slip surfaces having a variety of orientations, and each major orientation must be considered separately. Coulomb stress changes, induced by fault slip and resolved onto horizontal horizons above the fault, are calculated and shown in Figure 11. These calculations show the triggering effect of the blind thrust fault on superjacent layer interfaces. Localized frictional sliding along subhorizontal surfaces is promoted for layers located just above the fault tip, with the slip tendency decreasing with vertical distance above the fault tip. These calculations are analogous to those reported by *Cooke and Pollard* [1997] and *Roering et al.* [1997], who explicitly calculated the amount of frictional slip that would be triggered along particular interfaces. The calculations assume a larger value of frictional resistance ($\mu = 0.4$) for bedding planes than was used by *Niño et al.* [1998], who assumed extremely

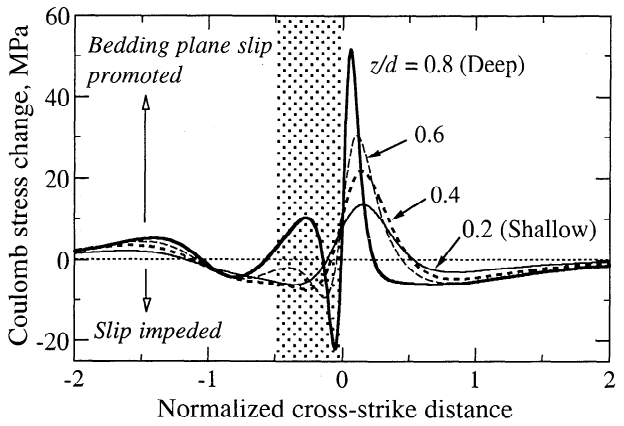

Figure 11. Localization of frictional sliding and bedding plane slip along horizontal planes as determined by changes in predicted Coulomb failure stress. Note that slip is promoted on layers closer to the upper tip of the blind fault (e.g., $z/d = 0.8$) to a greater degree than on those at progressively shallower depths.

weak (frictionless) interfaces in their models. Still larger values of frictional strength than used here (e.g., see *Cooke and Pollard*'s [1997] results for $\mu = 0.6$, and *Freed and Lin*'s [1998] results for $\mu = 0.8$) would promote folding in areas and at depths closer to the blind fault tip. These results demonstrate that slip along a blind thrust fault can nucleate bedding plane slip for a broader and more realistic range of interface strengths than was considered possible previously. Explicit mechanical modeling of the complete coupled system, using a range of plausible boundary conditions, is a fruitful area for future research.

8. Conclusions

A mechanical model of wrinkle ridges is developed in this paper. It postulates that wrinkle ridges grow as a result of slip along a subjacent blind thrust fault, and that bedding plane slip and backthrust faults are also localized above the blind fault. The model builds on previous kinematic hypotheses and motivates several key implications of wrinkle ridge development.

1. Wrinkle ridges can be interpreted as anticlinal folds of near-surface strata. The folds nucleate and grow in response to slip on a subjacent blind thrust fault. Previous folding-based models for wrinkle ridge growth (e.g., buckling) have been successful, in part, because they invoke bedding plane slip to form anticlines, a necessary ingredient for wrinkle ridge growth. However, the driving forces for folding in the present model include localized perturbations due to subjacent faulting, rather than a layer-parallel compression exclusively.

2. Kinematic models of folding can simulate the marginal slopes of wrinkle ridges whose topography has been quantified, supporting the interpretation of wrinkle ridges as anticlines. However, systematic variations in planimetric ridge width toward the tip regions, combined with suspected vertical topographic offsets across ridges, demonstrate for the first time that subjacent blind faults do not flatten and sole into regional décollements beneath wrinkle ridge terranes. Observations and models of terrestrial blind thrust faults indicate that bedding plane slip is critical for producing the wrinkle ridge morphologies investigated. However, frictional sliding along the subjacent thrust fault, instead of buckling or translation along a regional décollement, produces the flexure that is localized beneath the ridge by the fault.

3. The blind thrust model predicts that horizontal shortening of surface strata depends both on the position relative to the wrinkle ridge (in map view) and on the position relative to the blind thrust fault (in cross section). Estimates of shortening at the surface are significantly influenced by the depth of the blind thrust fault below the surface, leading to a depth dependence of the ratio of folding strains to faulting strains. However, the model predicts unambiguously that surface shortening is characteristically much less than that accommodated by the blind fault, providing the physical basis for comparable findings in the literature.

4. The magnitudes of both vertical uplift and horizontal shortening vary with position normal to a wrinkle ridge (as well as along its strike), with the most significant uplift developed above the location of the blind thrust fault plane. Assuming that wrinkle ridge width is approximately comparable to that of the subjacent blind fault, surface rocks within several ridge widths on either side of the wrinkle ridge should be affected by horizontal shortening, whereas vertical topography (uplift and/or subsidence) may extend to two to three ridge widths on either side. Topographic profiles (e.g., MOLA) should extend at least five ridge widths (or a total distance of >50 km) to adequately capture the total variation in offset topography associated with a wrinkle ridge. These particular values may become modified when results of explicit modeling of flexural slip folding, backthrust growth, and blind thrust faulting under far-field stress and displacement conditions become available. The region located between wrinkle ridges may reveal evidence for deformation due to nearby wrinkle ridges. Closely spaced ridges may interact mechanically over time, through stress changes associated with blind fault slip and anticline growth, to produce a population having distinctive statistical characteristics such as spacing and ridge width/length ratios.

5. Flexural slip folding initiates at depth above the blind fault's upper tip and propagates upward with increasing fault slip. The associated bedding plane slip is greatest near the fault tip, based on calculations of predicted Coulomb stress change, and can localize new backthrust faults given particular material properties that are conducive to strain softening. The tendency for bedding plane slip and backthrust fault localization to occur determines whether the blind thrust fault will be trapped at depth, promoting backthrust formation and leading to wrinkle ridge morphology, or will propagate to the surface, inhibiting backthrust formation and leading to lobate scarp morphology. Because wrinkle ridges require both flexural slip folding and thrust faulting to form, a combination of folding-based, faulting-based, and localized décollement (bedding plane slip) models is required for their formation.

Acknowledgments. This work was supported in part by grants from NASA's Planetary Geology and Geophysics Program to R.A.S. Comments on an earlier version by Vicki Hansen helped sharpen the clarity of the present paper. Thoughtful and thorough reviews by Tom Watters and an anonymous referee, and suggestions by Michele Cooke, improved the logic and cohesiveness of the final paper. Ross Stein kindly made available the COULOMB boundary element program and Jian Lin advised in its applications. Discussions with Michele Cooke, Jian Lin, Ken Tanaka, Tom Watters, Fernando Niño, Jean Chéry, Dominique Frizon de Lamotte, Nicolas Mangold, Daniel Mége, and Matt Golombek were also very helpful. Pleasant sabbatical stays at the Département de Géotectonique, Université Pierre et Marie Curie, Paris, and at Woods Hole Oceanographic Institution, helped to nurture and develop some of the ideas presented here. This is WHOI Contribution 10145.

References

Allemand, P., and P. Thomas, Modèle fragile des rides martiennes constraint par la géométrie de surface, *C. R. Acad. Sci. Paris, Sér. II, 215*, 1397–1402, 1992.

Aydin, A., Discontinuities along thrust faults and the cleavage duplexes, in *Geometries and Mechanisms of Thrusting, With Special Reference to the Appalachians*, edited by G. Mitra and S. Wojtal, *Spec. Pap. Geol. Soc. Am.*, *222*, 223–232, 1988.

Banerdt, W.B., M.P. Golombek, and K.L. Tanaka, Stress and tectonics on Mars, in *Mars*, edited by H.H. Kieffer, B.M. Jakosky, C.W. Snyder, and M.S. Matthews, pp. 249–297, Univ. of Ariz. Press, Tucson, 1992.

Barnett, J., J. Mortimer, J.H. Rippon, J.J. Walsh, and J. Watterson, Displacement geometry in the volume containing a single normal fault, *Am. Assoc. Petrol. Geol. Bull.*, *71*, 925–937, 1987.

Bilotti, F., and J. Suppe, The global distribution of wrinkle ridges on Venus, *Icarus*, *139*, 137–159, 1999.

Bruhn, R.L., and R.A. Schultz, Geometry and slip distribution in normal fault systems: Implications for mechanics and fault-related hazards, *J. Geophys. Res.*, *101*, 3401–3412, 1996.

Chester, J.S., J.M. Logan, and J.H. Spang, Influence of layering and boundary conditions on fault-bend and fault-propagation folding, *Geol. Soc. Am. Bull.*, *103*, 1059–1072, 1991.

Chicarro, A.F., P.H. Schultz, and P. Masson, Global and regional ridge patterns on Mars, *Icarus*, *63*, 153–174, 1985.

Chinnery, M.A., The deformation of the ground around surface faults, *Bull. Seismol. Soc. Am.*, *51*, 355–372, 1961.

Chinnery, M.A., The stress changes that accompany strike-slip faulting, *Bull. Seismol. Soc. Am.*, 53, 921–932, 1963.

Cohen, S.C., Postseismic deformation due to subcrustal viscoelastic relaxation following dip-slip earthquakes, *J. Geophys. Res.*, *89*, 4538–4544, 1984.

Cohen, S.C., Numerical models of crustal deformation in seismic zones, *Adv. Geophys.*, *41*, 133–231, 1999.

Colton, G.W., K.A. Howard, and H.J. Moore, Mare ridges and arches in southern Oceanus Procellarum, in Apollo 16 Preliminary Science Report, *NASA Spec. Publ.*, *SP–315*, 29-90–29-93, 1972.

Cooke, M.L., and D.D. Pollard, Bedding-plane slip in initial stages of fault-related folding, *J. Struct. Geol.*, *19*, 567–581, 1997.

Cowie, P.A., and C.H. Scholz, Displacement-length scaling relationship for faults: Data synthesis and discussion, *J. Struct. Geol.*, *14*, 1149–1156, 1992.

Crider, J.G., and D.D. Pollard, Fault linkage: Three-dimensional mechanical interaction between echelon normal faults, *J. Geophys. Res.*, *103*, 24,373–24,391, 1998.

Crouch, S.L., and A.M. Starfield, *Boundary Element Methods in Solid Mechanics*, 322 pp., Allen and Unwin, Winchester, Mass., 1983.

Currie, J.B., H.W. Patnode, and R.P. Trump, Development of folds in sedimentary strata, *Geol. Soc. Am. Bull.*, *73*, 655–674, 1962.

Davison, I., Linked fault systems; extensional, strike-slip and contractional, in *Continental Deformation*, edited by P.L. Hancock, pp. 121–142, Pergamon, Tarrytown, N.Y., 1994.

Erickson, S.G., Influence of mechanical stratigraphy on folding vs. faulting, *J. Struct. Geol.*, *18*, 443–450, 1996.

Fletcher, R.C., and D.D. Pollard, Can we understand structural and tectonic processes and their products without appeal to a complete mechanics?, *J. Struct. Geol.*, *21*, 1071–1088, 1999.

Freed, A.M., and J. Lin, Time-dependent changes in failure stress following thrust earthquakes, *J. Geophys. Res.*, *103*, 24,393–24,409, 1998.

Geiser, P.A., The role of kinematics in the construction and analysis of geological cross sections in deformed terranes, in *Geometries and Mechanisms of Thrusting, With Special Reference to the Appalachians*, edited by G. Mitra and S. Wojtal, *Spec. Pap. Geol. Soc. Am.*, *222*, 47–76, 1988.

Golombek, M.P., and W.B. Banerdt, Recent advances in Mars tectonics (abstract), *Int. Conf. Mars* [CD-ROM], *5th*, abstract 6020, 1999.

Golombek, M.P., J. Suppe, W. Narr, J. Plescia, and B. Banerdt, Involvement of the lithosphere in the formation of wrinkle ridges on Mars (abstract), in MEVTV Workshop on Tectonic Features on Mars, edited by T.R. Watters and M.P. Golombek, *LPI Tech. Rep. 89–06*, pp. 12–14, Lunar and Planet. Inst., Houston, Tex., 1989.

Golombek, M.P., J.B. Plescia, and B.J. Franklin, Faulting and folding in the formation of planetary wrinkle ridges, *Proc. Lunar Planet. Sci. Conf.*, *21st*, 679–693, 1991.

Golombek, M.P., W.B. Banerdt, K.L. Tanaka, and D.M. Tralli, A prediction of Mars seismicity from surface faulting, *Science*, *258*, 979–981, 1992.

Golombek, M.P., F.S. Anderson, and M.T. Zuber, Topographic profiles across wrinkle ridges indicate subsurface faults (abstract), *Eos Trans. AGU*, Fall Meet. Suppl., *80*(46), F610, 1999.

Golombek, M.P., F.S. Anderson, and M.T. Zuber, Martian wrinkle ridge topography: Evidence for subsurface faults from MOLA (abstract), *Lunar Planet. Sci.* [CD-ROM], *XXXI*, abstract 1294, 2000.

Harris, R.A., Introduction to the special section: Stress triggers, stress shadows, and implications for seismic hazard, *J. Geophys. Res.*, *103*, 24,347–24,358, 1998.

Harris, R.A., and R.W. Simpson, Changes in static failure stress on southern California faults after the 1992 Landers earthquake, *Nature*, *360*, 251–254, 1992.

Hill, M.L., Earthquakes and folding, Coalinga, California, *Geology*, *12*, 711–712, 1984.

Howard, K.A., and W.R. Muehlberger, Lunar thrust faults in the Taurus-Littrow region, in Apollo 17 Preliminary Science Report, *NASA Spec. Publ.*, *SP–330*, 31-12–31-21, 1973.

Jamison, W.R., Fault-fracture strain in Wingate sandstone, *J. Struct. Geol.*, *11*, 959–974, 1989.

Johnson, A.M., Folding and faulting of strain-hardening sedimentary rocks, *Tectonophysics*, *62*, 251–278, 1980.

Johnson, A.M., and R.C. Fletcher, *Folding of Viscous Layers*, 461 pp., Columbia Univ. Press, New York, 1994.

King, G., and G. Yielding, The evolution of a thrust system: Processes of rupture initiation, propagation and termination in the 1980 El Asnam (Algeria) earthquake, *Geophys. J. R. Astron. Soc.*, *77*, 915–933, 1984.

King, G.C.P., R.S. Stein, and J.B. Rundle, The growth of geological structures by repeated earthquakes, 1, Conceptual framework, *J. Geophys. Res.*, *93*, 13,307–13,318, 1988.

King, G.C.P., R.S. Stein, and J. Lin, Static stress changes and the triggering of earthquakes, *Bull. Seismol. Soc. Am.*, *84*, 935–953, 1994.

Kreslavsky, M.A., and A.T. Basilevsky, Morphometry of wrinkle ridges on Venus: Comparison with other planets, *J. Geophys. Res.*, *103*, 11,103–11,111, 1998.

Li, V.C., Mechanics of shear rupture applied to earthquake zones, in *Fracture Mechanics of Rock*, edited by B.K. Atkinson, pp. 351–428, Academic, San Diego, Calif., 1987.

Lin, J., and R.S. Stein, Coseismic folding, earthquake recurrence, and the 1987 source mechanism at Whittier Narrows, Los Angeles basin, California, *J. Geophys. Res.*, *94*, 9614–9632, 1989.

Lucchitta, B.K., Mare ridges and related highland scarps: Results of vertical tectonism?, *Proc. Lunar Sci. Conf.*, *7th*, 2761–2782, 1976.

Lucchitta, B.K., Topography, structure, and mare ridges in southern Mare Imbrium and northern Oceanus Procellarum, *Proc. Lunar Sci. Conf.*, *8th*, 2691–2703, 1977.

Lucchitta, B.K., and J.L. Klockenbrink, Ridges and scarps in the equatorial belt of Mars, *Moon Planets*, *24*, 415–429, 1981.

Ma, X.Q., and N.J. Kusznir, 3-D subsurface displacement and strain fields for faults and fault arrays in a layered elastic half-space, *Geophys. J. Int.*, *111*, 542–558, 1992.

Ma, X.Q., and N.J. Kusznir, Modelling of near-field subsurface displacements for generalized faults and fault arrays, *J. Struct. Geol.*, *15*, 1471–1484, 1993.

MacKinnon, D.J., and K.L. Tanaka, The impacted Martian crust: Structure, hydrology, and some geologic implications, *J. Geophys. Res.*, *94*, 17,359–17,370, 1989.

Malin, M.C., and K.S. Edgett, MGS MOC the first year: Geomorphic processes and landforms (abstract), *Lunar Planet. Sci.*, *XXX*, #1028 (on CD-ROM), 1999.

Malin, M.C., et al., Early views of the Martian surface from the Mars Orbiter Camera of Mars Global Surveyor, *Science*, *279*, 1681–1685, 1998.

Mangold, N., Rhéologie du perigélisol de Mars: Applications géomorphologiques et structurales, conséquences sur l'origine des constraintes compressives, Ph.D. thesis, 238 pp., Ecole Normale Supérieure de Lyon et Univ. Claude Bernard Lyon I, Lyon, France, Dec. 1997.

Mangold, N., P. Allemand, and P.G. Thomas, Wrinkle ridges of Mars: Structural analysis and evidence for shallow deformation controlled by ice-rich décollements, *Planet. Space Sci.*, *46*, 345–356, 1998.

Mansinha, L., and D.E. Smylie, The displacement fields of inclined faults, *Bull. Seismol. Soc. Am.*, *61*, 1433–1440, 1971.

Martel, S.J., and D.D. Pollard, Mechanics of slip and fracture along small faults and simple strike-slip fault zones in granitic rock, *J. Geophys. Res.*, *94*, 9417–9428, 1989.

Maxwell, T.A., F. El-Baz, and S.H. Ward, Distribution, morphology, and origin of ridges and arches in Mare Serenitatis, *Geol. Soc. Am. Bull.*, *86*, 1273–1278, 1975.

McEwen, A.S., M.C. Malin, M.H. Carr, and W.K. Hartmann, Voluminous

volcanism on early Mars revealed in Valles Marineris, *Nature*, *397*, 584–586, 1999.

McGill, G.E., Wrinkle ridges, stress domains, and kinematics of Venusian plains, *Geophys. Res. Lett.*, *20*, 2407–2410, 1993.

Melosh, H.J., Vertical movements following a dip-slip earthquake, *Geophys. Res. Lett.*, *10*, 47–50, 1983.

Mercier, E., F. Outtani, and D. Frizon de Lamotte, Late-stage evolution of fault-propagation folds: Principles and example, *J. Struct. Geol.*, *19*, 185–193, 1997.

Mitra, G., and A.J. Sussman, Structural evolution of connecting splay duplexes and their implications for critical taper: An example based on geometry and kinematics of the Canyon Range culmination, Sevier Belt, central Utah, *J. Struct. Geol.*, *19*, 503–521, 1997.

Mitra, S., Fault-propagation folds: Geometry, kinematic evolution, and hydrocarbon traps, *Am. Assoc. Petrol. Geol. Bull.*, *74*, 921–945, 1990.

Mitra, S., and V.S. Mount, Foreland basement-involved structures, *Am. Assoc. Petrol. Geol. Bull.*, *82*, 70–109, 1998. (Errata, *Am. Assoc. Petrol. Geol. Bull.*, *83*, 2024–2027, 1999.)

Mitra, S., and V.S. Mount, Foreland basement-involved structures: Reply, *Am. Assoc. Petrol. Geol. Bull.*, *83*, 2017–2023, 1999.

Montési, L.G.J., M.T. Zuber, and O. Aharonson, Geometry of faults underlying wrinkle ridges on Mars: Dynamic modeling and MOLA topography (abstract), *Lunar Planet. Sci.* [CD-ROM], *XXXI*, abstract 1927, 2000.

Mouginis-Mark, P.J., L. Wilson, and M.T. Zuber, The physical volcanology of Mars, in *Mars*, edited by H.H. Kieffer, B.M. Jakosky, C.W. Snyder, and M.S. Matthews, pp. 424–452, Univ. of Ariz. Press, Tucson, 1992.

Muehlberger, W.R., Structural history of southeastern Mare Serenitatis and adjacent highlands, *Proc. Lunar Sci. Conf., 5th*, 101–110, 1974.

Niño, F., H. Philip, and J. Chéry, The role of bed-parallel slip in the formation of blind thrust faults, *J. Struct. Geol.*, *20*, 503–516, 1998.

Okada, Y., Internal deformation due to shear and tensile faults in a half-space, *Bull. Seismol. Soc. Am.*, *82*, 1018–1040, 1992.

Perfettini, H., R.S. Stein, R. Simpson, and M. Cocco, Stress transfer by the 1988–1989 M=5.3 and 5.4 Lake Elsman foreshocks to the Loma Prieta fault: Unclamping at the site of peak mainshock slip, *J. Geophys. Res.*, *104*, 20,169–20,182, 1999.

Philip, H., and M. Meghraoui, Structural analysis and interpretation of the surface deformations of the El Asnam earthquake of October 10, 1980, *Tectonics*, *2*, 17–49, 1983.

Philip, H., E. Rogozhin, A. Cisternas, J.C. Bousquet, B. Borisov, and A. Karakhanian, The Armenian earthquake of 1988, December 7: Faulting and folding, neotectonics and paleoseismicity, *Geophys. J. Int.*, *110*, 141–158, 1992.

Plescia, J.B., Wrinkle ridges in Lunae Planum, Mars: Implications for shortening and strain, *Geophys. Res. Lett.*, *18*, 913–916, 1991.

Plescia, J.B., Wrinkle ridges of Arcadia Planitia Mars, *J. Geophys. Res.*, *98*, 15,049–15,059, 1993.

Plescia, J.B., and M.P. Golombek, Origin of planetary wrinkle ridges based on the study of terrestrial analogs, *Geol. Soc. Am. Bull.*, *97*, 1289–1299, 1986.

Pollard, D.D., and P. Segall, Theoretical displacements and stresses near fractures in rock: With applications to faults, joints, veins, dikes, and solution surfaces, in *Fracture Mechanics of Rock*, edited by B.K. Atkinson, pp. 277–349, Academic, San Diego, Calif., 1987.

Price, N.J., and J.W. Cosgrove, *Analysis of Geological Structures*, 502 pp., Cambridge Univ. Press, New York, 1990.

Reidel, S.P., T.L. Tolan, P.R. Hooper, K.R. Fecht, M.H. Beeson, R.D. Bentley, and J.L. Anderson, The Grande Ronde Basalt, Columbia River Basalt Group: Stratigraphic descriptions and correlations in Washington, Oregon, and Idaho, in *Volcanism and Tectonism in the Columbia River Flood-Basalt Province*, edited by S.P. Reidel and P.R. Hooper, *Spec. Pap. Geol. Soc. Am.*, *238*, 21–53, 1989.

Rispoli, R., Stress fields about strike-slip faults inferred from stylolites and tension gashes, *Tectonophysics*, *75*, T29–T36, 1981.

Roering, J.J., M.L. Cooke, and D.D. Pollard, Why blind thrust faults do not propagate to the Earth's surface: Numerical modeling of coseismic deformation associated with thrust-related anticlines, *J. Geophys. Res.*, *102*, 11,901–11,912, 1997.

Rudnicki, J.W., Fracture mechanics applied to the Earth's crust, *Annu. Rev. Earth Planet. Sci.*, *8*, 489–525, 1980.

Ruegg, J.C., M. Kasser, A. Tarantola, L.C. Lepine, and B. Chouikrat, Deformations associated with the El Asnam earthquake of October 1980: Geodetic determination of vertical and horizontal movements, *Bull. Seismol. Soc. Am.*, *72*, 2227–2244, 1982.

Rundle, J.B., Viscoelastic-gravitational deformation by a rectangular thrust fault in a layered Earth, *J. Geophys. Res.*, *87*, 7787–7796, 1982.

Saunders, R.S., and T.E. Gregory, Tectonic implications of Martian ridged plains (abstract), in Reports of Planetary Geology and Geophysics Program, 1980, *NASA Tech. Memo.*, *TM–82385*, 93–94, 1980.

Savage, J.C., and L.M. Hastie, Surface deformation associated with dip-slip faulting, *J. Geophys. Res.*, *71*, 4897–4904, 1966.

Schultz, P.H., *Moon Morphology*, 626 pp., Univ. of Tex. Press, Austin, 1976.

Schultz, P.H., R.A. Schultz, and J.L. Rogers, The structure and evolution of ancient impact basins on Mars, *J. Geophys. Res.*, *87*, 9803–9820, 1982.

Schultz, R.A., Relative scale and the strength and deformability of rock masses, *J. Struct. Geol.*, *18*, 1139–1149, 1996.

Schultz, R.A., Displacement-length scaling for terrestrial and Martian faults: Implications for Valles Marineris and shallow planetary grabens, *J. Geophys. Res.*, *102*, 12,009–12,015, 1997.

Schultz, R.A., Understanding the process of faulting: Selected challenges and opportunities at the edge of the 21st century, *J. Struct. Geol.*, *21*, 985–993, 1999.

Schultz, R.A., Fault-population statistics at the Valles Marineris Extensional Province, Mars: Implications for segment linkage, crustal strains, and its geodynamic development, *Tectonophysics*, *316*, 169–193, 2000.

Schultz, R.A., and H.V. Frey, A new survey of multiring impact basins on Mars, *J. Geophys. Res.*, *95*, 14,175–14,189, 1990.

Schultz, R.A., and K.L. Tanaka, Lithospheric-scale buckling and thrust structures on Mars: The Coprates rise and south Tharsis ridge belt, *J. Geophys. Res.*, *99*, 8371–8385, 1994.

Schultz, R.A., and T.R. Watters, Elastic buckling of fractured basalt on the Columbia Plateau, Washington, in *Rock Mechanics: Proceedings of the 35th U.S. Symposium*, edited by J.J.K. Daemen and R.A. Schultz, pp. 855–860, A.A. Balkema, Brookfield, Vt., 1995.

Segall, P., and D.D. Pollard, Mechanics of discontinuous faults, *J. Geophys. Res.*, *85*, 4337–4350, 1980.

Sharpton, V.L., and J.W. Head, Lunar mare ridges: Analysis of ridge-crater intersections and implications for the tectonic origin of mare ridges, *Proc. Lunar Planet. Sci. Conf., 18th*, 307–317, 1988.

Shaw, J.H., and J. Suppe, Earthquake hazards of active blind-thrust faults under the central Los Angeles basin, California, *J. Geophys. Res.*, *101*, 8623–8642, 1996.

Shaw, J.H., F. Bilotti, and P.A. Brennan, Patterns of imbricate thrusting, *Geol. Soc. Am. Bull.*, *111*, 1140–1154, 1999.

Sibson, R.H., An assessment of field evidence for 'Byerlee' friction, *Pure Appl. Geophys.*, *142*, 645–662, 1994.

Smith, D.E., et al., The global topography of Mars and implications for surface evolution, *Science*, *284*, 1495–1503, 1999.

Stein, R.S., and G.C.P. King, Seismic potential revealed by folding: 1983 Coalinga, California, earthquake, *Science*, *224*, 869–872, 1984.

Stein, R.S., G.C. King, and J.B. Rundle, The growth of geological structures by repeated earthquakes, 2, Field examples of continental dip-slip faults, *J. Geophys. Res.*, *93*, 13,319–13,331, 1988.

Stein, R.S., G.C.P. King, and J. Lin, Change in failure stress on the southern San Andreas Fault system caused by the 1992 magnitude = 7.4 Landers earthquake, *Science*, *258*, 1328–1332, 1992.

Stein, R.S., G.C.P. King, and J. Lin, Stress triggering of the 1994 M=6.7 Northridge, California, earthquake by its predecessors, *Science*, *265*, 1432–1435, 1994.

Stone, D.S., Forcland basement-involved structures: Discussion, *Am. Assoc. Petrol. Geol. Bull.*, *83*, 2006–2016, 1999.

Strom, R.G., Lunar mare ridges, rings and volcanic ring complexes, *Mod. Geol.*, *2*, 133–157, 1972.

Strom, R.G., N.J. Trask, and J.E. Guest, Tectonism and volcanism on Mercury, *J. Geophys. Res.*, *80*, 2478–2507, 1975.

Suppe, J., Geometry and kinematics of fault-bend folding, *Am. J. Sci.*, *283*, 648–721, 1983.

Suppe, J., and C. Connors, Critical taper wedge mechanics of fold-and-thrust belts on Venus: Initial results from Magellan, *J. Geophys. Res.*, *97*, 13,545–13,561, 1992.

Suppe, J., and D. Medwedeff, Geometry and kinematics of fault propagation folding, *Eclogae Geol. Helv.*, 83, 409–454, 1990.

Suppe, J., and W. Narr, Fault-related folding on the Earth with application to wrinkle ridges on Mars and the Moon (abstract), in MEVTV Workshop on Tectonic Features on Mars, edited by T.R. Watters and M.P. Golombek, *LPI Tech. Rep. 89–06*, pp. 29–30, Lunar and Planet. Inst., Houston, Tex., 1989.

Taboada, A., J.C. Bousquet, and H. Philip, Coseismic elastic models of

folds above blind thrusts in the Betic Cordilleras (Spain) and evaluation of seismic hazard, *Tectonophysics*, *220*, 223–241, 1993.

Tanaka, K.L., M.P. Golombek, and W.B. Banerdt, Reconciliation of stress and structural histories of the Tharsis region of Mars, *J. Geophys. Res.*, *96*, 15,617–15,633, 1991.

Toda, S., R.S. Stein, P.A. Reasenberg, J.H. Dieterich, and A. Yoshida, Stress transferred by the 1995 Mw=6.9 Kobe, Japan, shock: Effect on aftershocks and future earthquake probabilities, *J. Geophys. Res.*, *103*, 24,543–24,565, 1998.

Watters, T.R., Wrinkle ridge assemblages on the terrestrial planets, *J. Geophys. Res.*, *93*, 10,236–10,254, 1988.

Watters, T.R., Periodically spaced anticlines of the Columbia Plateau, in *Volcanism and Tectonism in the Columbia River Flood-Basalt Province*, edited by S.P. Reidel and P.R. Hooper, *Spec. Pap. Geol. Soc. Am.*, *238*, 283–292, 1989.

Watters, T.R., Origin of periodically spaced wrinkle ridges on the Tharsis Plateau of Mars, *J. Geophys. Res.*, *96*, 15,599–15,616, 1991.

Watters, T.R., Compressional tectonism on Mars, *J. Geophys. Res.*, *98*, 17,049–17,060, 1993.

Watters, T.R., and M.S. Robinson, Radar and photoclinometric studies of wrinkle ridges on Mars, *J. Geophys. Res.*, *102*, 10,889–10,903, 1997.

Watters, T.R., and M.S. Robinson, Topographic studies of wrinkle ridges: The significance of elevation offsets (abstract), *Lunar Planet. Sci.* [CD-ROM], *XXXI*, abstract 1879, 2000.

Watters, T.R., M.S. Robinson, and A.C. Cook, Topography of lobate scarps on Mercury: New constraints on the planet's contraction, *Geology*, *26*, 991–994, 1998.

West, M.W., F.X. Ashland, A.J. Busacca, G.W Berger, and M.E. Shaffer, Late Quaternary deformation, Saddle Mountains anticline, south-central Washington, *Geology*, *24*, 1123–1126, 1996.

Willemse, E.J.M., and D.D. Pollard, On the orientation and patterns of wing cracks and solution surfaces at the tips of a sliding flaw or fault, *J. Geophys. Res.*, *103*, 2427–2438, 1998.

Williams, C.A., C. Connors, F.A. Dahlen, E.J. Price, and J. Suppe, Effect of the brittle-ductile transition on the topography of compressive mountain belts on Earth and Venus, *J. Geophys. Res.*, *99*, 19,947–19,974, 1994.

Wojtal, S.F., Measuring displacement gradients and strains in faulted rocks, *J. Struct. Geol.*, *11*, 669–678, 1989.

Woodcock, N.H., and M. Fischer, Strike-slip duplexes, *J. Struct. Geol.*, *8*, 725–735, 1986.

Zuber, M.T., Wrinkle ridges, reverse faulting, and the depth penetration of lithospheric strain in Lunae Planum Mars, *Icarus*, *114*, 80–92, 1995.

Zuber, M.T., and L.L. Aist, The shallow structure of the Martian lithosphere in the vicinity of the ridged plains, *J. Geophys. Res.*, *95*, 14,215–14,230, 1990.

R.A. Schultz, Geomechanics–Rock Fracture Group, Department of Geological Sciences/172, Mackay School of Mines, University of Nevada, Reno NV 89557–0138. (schultz@mines.unr.edu)

(Received November 1, 1999; revised February 22, 2000;
accepted February 29, 2000.)